JCB

Article

Structure–function insights into direct lipid transfer between membranes by Mmm1–Mdm12 of ERMES

Shin Kawano,[1,2,4,5] Yasushi Tamura,[5,6,8] Rieko Kojima,[8] Siqin Bala,[4] Eri Asai,[4] Agnès H. Michel,[9] Benoît Kornmann,[9] Isabelle Riezman,[10] Howard Riezman,[10] Yoshitake Sakae,[7] Yuko Okamoto,[7] and Toshiya Endo[1,2,3,4,5]

[1]Faculty of Life Sciences, [2]Japan Science and Technology Agency/Core Research for Evolutional Science and Technology, and [3]Institute for Protein Dynamics, Kyoto Sangyo University, Kyoto, Japan
[4]Department of Chemistry, Graduate School of Science, [5]Japan Science and Technology Agency/Core Research for Evolutional Science and Technology, [6]Research Center for Materials Science, and [7]Department of Physics, Graduate School of Science, Nagoya University, Nagoya, Japan
[8]Department of Material and Biological Chemistry, Faculty of Science, Yamagata University, Yamagata, Japan
[9]Institute of Biochemistry, ETH Zürich, Zürich, Switzerland
[10]Department of Biochemistry, National Centre of Competence in Research Chemical Biology, University of Geneva, Geneva, Switzerland

The endoplasmic reticulum (ER)–mitochondrial encounter structure (ERMES) physically links the membranes of the ER and mitochondria in yeast. Although the ER and mitochondria cooperate to synthesize glycerophospholipids, whether ERMES directly facilitates the lipid exchange between the two organelles remains controversial. Here, we compared the x-ray structures of an ERMES subunit Mdm12 from *Kluyveromyces lactis* with that of Mdm12 from *Saccharomyces cerevisiae* and found that both Mdm12 proteins possess a hydrophobic pocket for phospholipid binding. However in vitro lipid transfer assays showed that Mdm12 alone or an Mmm1 (another ERMES subunit) fusion protein exhibited only a weak lipid transfer activity between liposomes. In contrast, Mdm12 in a complex with Mmm1 mediated efficient lipid transfer between liposomes. Mutations in Mmm1 or Mdm12 impaired the lipid transfer activities of the Mdm12–Mmm1 complex and furthermore caused defective phosphatidylserine transport from the ER to mitochondrial membranes via ERMES in vitro. Therefore, the Mmm1–Mdm12 complex functions as a minimal unit that mediates lipid transfer between membranes.

Introduction

Eukaryotic cells are compartmentalized into membrane-bound organelles, each of which performs distinct biochemical tasks. However, the recent identification of direct physical contacts between the membranes of two organelles (Kornmann et al., 2009; Elbaz-Alon et al., 2014; Hönscher et al., 2014; Lahiri et al., 2014; Murley et al., 2015) highlights the need for coordinated functions of distinct organelles through direct exchange of metabolites and information. The ER-mitochondrial encounter structure (ERMES) is one such interorganelle tethering entity, and it physically links the membranes of the ER and mitochondria in yeast cells (Kornmann et al., 2009).

ERMES consists of four core subunits: Mmm1, an N-anchor ER membrane protein (Burgess et al., 1994); Mdm10, a β-barrel mitochondrial outer membrane (OM) protein (Sogo and Yaffe, 1994); Mdm34/Mmm2, an OM protein without an obvious transmembrane segment (Youngman et al., 2004), and Mdm12, a peripheral OM protein (Berger et al., 1997). ERMES also consists of the peripheral components Gem1 (Frederick et al., 2004; Kornmann et al., 2011; Stroud et al., 2011) and Tom7 (Yamano et al., 2010). ERMES was proposed to facilitate lipid exchange between the ER and mitochondria (Kornmann et al., 2009). Because most phospholipid biosynthetic pathways are present in the ER and mitochondria, production of cellular phospholipids relies on efficient transport of their precursor lipids between these organelles (Scharwey et al., 2013; Tamura et al., 2014; Tatsuta and Langer, 2017). For instance, cardiolipin, a mitochondrial signature phospholipid, is generated in the mitochondrial inner membrane from phosphatidic acid (PA), a precursor phospholipid that is supplied by the ER. Similarly, phosphatidylserine (PS) generated in the ER is transported to mitochondria, where it is converted to phosphatidylethanolamine (PE). PE is then transported back from mitochondria to the ER and methylated to form phosphatidylcholine (PC). Three ERMES subunits (Mmm1, Mdm12, and Mdm34) contain a synaptotagmin-like mitochondrial lipid-binding protein (SMP) domain, which may belong to the TULIP superfamily (Kopec et al., 2010, 2011), suggesting that these proteins can bind to phospholipids. Indeed, the purified SMP domain of yeast Mdm12 and that of Mmm1 fused to maltose-binding protein (MBP) were shown to bind to phospholipids (AhYoung et al., 2015; Jeong et al., 2016). However, there is no compelling evidence for ERMES mediating direct lipid transfer between membranes.

Correspondence to Toshiya Endo: tendo@cc.kyoto-su.ac.jp

The Rockefeller University Press
J. Cell Biol. Vol. 217 No. 3 959–974
https://doi.org/10.1083/jcb.201704119

Recently developed in vitro phospholipid transport assays using isolated membranes mainly derived from mitochondria and the ER revealed that lack of an ERMES component (e.g., Mmm1, Mdm12, or Mdm34) impairs PS transport from the ER to mitochondria, but not PE transport from mitochondria to the ER (Kojima et al., 2016). Mutations or deletions of ERMES components lead to altered morphology and/or cellular lipid composition (Dimmer et al., 2002; Kornmann et al., 2009; Osman et al., 2009; Nguyen et al., 2012; Tamura et al., 2012; Voss et al., 2012; Tan et al., 2013). Nevertheless, it is still difficult to judge whether ERMES directly mediates phospholipid transport between organelles or defects in other ERMES functions, like the shape of the ER and/or mitochondria, indirectly affect lipid exchange. Further complicating the interpretation is that an increase in other ER–mitochondria contacts and/or expansion of the area of the ER–vacuole contact region may compensate for a loss of ERMES (Elbaz-Alon et al., 2014, 2015; Lahiri et al., 2014; Lang et al., 2015; Murley et al., 2015). Therefore, a possible lipid transfer function of ERMES at ER–mitochondrial contact sites has not been clearly established yet.

Structural information on ERMES subunits became available only recently. On the basis of a 17-Å-resolution electron microscopy image, AhYoung et al. (2015) constructed a model of the complex between Mmm1 and Mdm12 as a central (likely head [Mmm1]-to-head [Mmm1]) dimer flanked by two molecules of Mdm12 in a tail (Mmm1)-to-head (Mdm12) arrangement. Jeong et al. (2016) determined a 3.1-Å-resolution x-ray structure of *Saccharomyces cerevisiae* Mdm12, which formed a head-to-head interlocking dimer through domain swapping of the N-terminal β-strand, yet they proposed a provocative model in which the Mdm12 dimer dissociates into a monomer to associate with a head (Mmm1)-to-head (Mmm1) dimer of Mmm1 (likely in a tail [Mmm1]-to-tail [Mdm12] arrangement) and with Mdm34 in a head (Mdm12)-to-head (Mdm34) interlocking manner. In this study, we determined the x-ray structures of Mdm12 from *Kluyveromyces lactis* and found that interlocking homodimer formation does not play an important role in Mdm12 function. We further demonstrated that Mdm12 or Mmm1 alone is only marginally active in lipid transfer, but the Mmm1–Mdm12 complex exerts efficient phospholipid transfer between membranes in vitro. These results support a model in which ERMES is responsible for not only membrane tethering but also facilitating efficient lipid exchange at ER–mitochondria contact sites, and the Mmm1–Mdm12 pair is central in the lipid transfer function of ERMES.

Results

Comparison of the phospholipid-bound structures between *K. lactis* and *S. cerevisiae* Mdm12

Mdm12 from yeast *K. lactis* is homologous in its amino acid sequence to Mdm12 from *S. cerevisiae* (Fig. S1) and can functionally replace *S. cerevisiae* Mdm12 in *S. cerevisiae* cells (Fig. 1 A). To gain insight into the functions of Mdm12, we crystallized and determined the structures of the *K. lactis* Mdm12 core protein lacking nonconserved C-terminal residues (residues 1–239, KlMdm12) at 3.1 Å resolution, its dimethyllysine modified form (KlMdm12dmLys) at 2.25 Å resolution, and *K. lactis* full-length Mdm12 (residues 1–305, KlMdm12FL) at 3.5 Å resolution (Figs. S2 and S3 and Table 1), and we compared them with that of Mdm12 from *S. cerevisiae* at 3.1 Å resolution (ScMdm12; Fig. S3; Jeong et al., 2016). The crystal structures of the *K. lactis* Mdm12 derivatives are essentially identical, except for the N-terminal and/or C-terminal segment (Fig. S3, A and B), and we hereafter refer to the Mdm12dmLys structure with the highest resolution as the KlMdm12 structure. The overall folding of KlMdm12 exhibits an inverted cone-like structure, which is similar to that of ScMdm12 (Fig. S3 C), reflecting their amino acid sequence similarities (Fig. S1). The nonconserved regions (residues 67–85 of KlMdm12 and residues 70–114 of ScMdm12; Fig. S3 A) are disordered in the determined structures.

The ScMdm12 structure has a hydrophobic cavity with a crevice-like opening that spans the "base" and "edge" of the cone-shaped structure, in which bound diacyl glycerophospholipid was identified (Fig. S3 D; Jeong et al., 2016). The determined KlMdm12 structure also revealed the presence of a hydrophobic pocket mainly consisting of conserved hydrophobic residues in which bound phospholipid was unambiguously located (Figs. S1 and S4 A). Although the presence of a deep hydrophobic cavity for phospholipid binding is common to ScMdm12 and KlMdm12, there are significant differences in the positions of the openings of the hydrophobic cavities and bound lipid conformations between ScMdm12 and KlMdm12, which are shown in Fig. S3 (D–G). In particular, KlMdm12 has an opening at the base, but not the edge, of the cone-shaped structure (Fig. S3 E), so that the head group of the bound lipid is located at the pocket opening at the base.

In vitro lipid transfer assays using mitochondria and ER membranes showed that ERMES primarily transports PS, not PE, between the ER and mitochondria (Kojima et al., 2016). TLC analyses revealed that the lipids extracted from the recombinant KlMdm12 purified from *E. coli* cells were PE and PG, two of the major *E. coli* phospholipids (Fig. S4 B), suggesting that KlMdm12 can bind to phospholipids with no significant preference between PE and PG, but not to cardiolipin with four acyl chains, in *E. coli* cells (*E. coli* cells lack PC). Mass spectrometry analysis of lipids bound to recombinant ScMdm12 expressed in *E. coli* cells also showed that ScMdm12 does not have strong preference for acyl-chain length for binding (Fig. S4 C). Studies using in vitro lipid displacement assays and/or mass spectrometry analyses of bound lipids in *S. cerevisiae* cells have reported a moderate lipid binding preference of PC (and PG) to PA and to PS for ScMdm12 (AhYoung et al., 2015; Jeong et al., 2016). This weak substrate specificity for neutral phospholipid PC as compared with acidic phospholipids was ascribed to the acidic residues near the opening of the hydrophobic cavity at the edge of the corn, where the head group of the bound lipid is located (Fig. S3 E; Jeong et al., 2016). However, in contradiction to this proposal, the opening of the hydrophobic pocket in KlMdm12 at the base of the corn exhibits only limited presence of net negative charges (Fig. S3 H).

To test whether the structural properties of the lipid-binding pocket, including its opening, change upon removal of the lipid in KlMdm12, we produced dimethyl-lysine–modified KlMdm12 crystals in the presence of a detergent (FOS-MEA-10), which removed most bound lipid molecules from KlMdm12, and determined the structure of lipid-free Mdm12 at 3.3 Å resolution (Table 1 and Fig. S4 D). Although structural flexibility reflected in the crystallographic temperature factors and disordered residues (Fig. S4, A and D) was larger for lipid-free KlMdm12 than lipid-bound KlMdm12, the overall

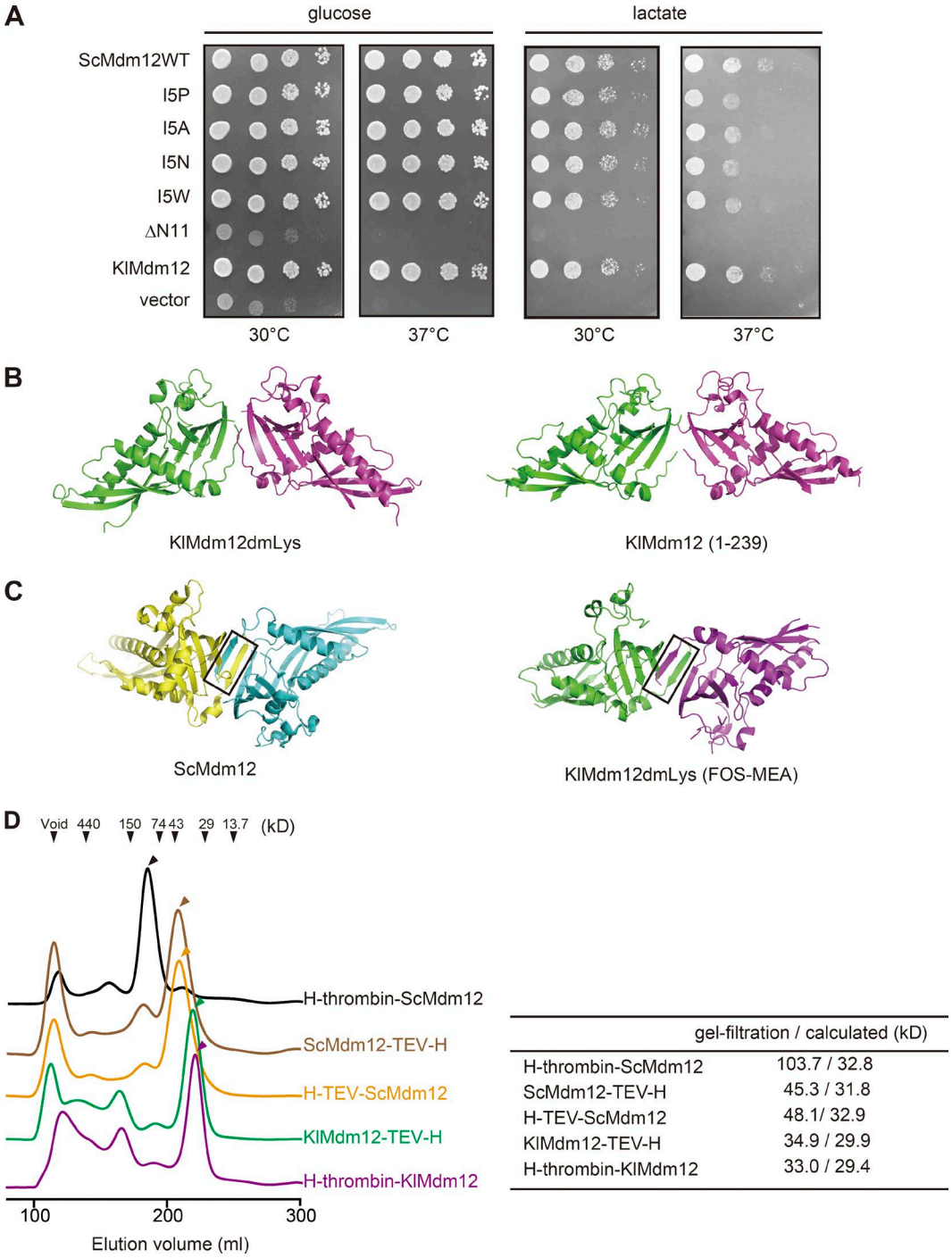

	gel-filtration / calculated (kD)
H-thrombin-ScMdm12	103.7 / 32.8
ScMdm12-TEV-H	45.3 / 31.8
H-TEV-ScMdm12	48.1/ 32.9
KlMdm12-TEV-H	34.9 / 29.9
H-thrombin-KlMdm12	33.0 / 29.4

Figure 1. **Oligomer formation and lipid binding of Mdm12. (A)** A pRS314 vector containing the gene for ScMdm12 (ScMdm12WT); ScMdm12 with the mutation of I5P, I5A, I5N, or I5W; ScMdm12 lacking the N-terminal 11 residues (ΔN11); or KlMdm12(1–239) was introduced into the *S. cerevisiae mdm12*Δ strain by plasmid shuffling. An empty pR314 vector was introduced into the *mdm12*Δ strain as a control (vector). Saturated cultures of the indicated cells were diluted with 10-fold increments, spotted on SCD (–Trp, +FOA) or SCLac (–Trp, +FOA) plates, and incubated at 30°C or 37°C for 2 or 3 d, respectively. **(B)** Dimeric arrangement found in the crystal structures of KlMdm12. Structures of KlMdm12(1–239), residues 1–239 of KlMdm12 without modification (left), and KlMdm12dmLys, dimethyl-lysine–modified KlMdm12(1–239) (right) are shown in ribbon form. **(C)** Interlocking dimers found in ScMdm12 (left; Jeong et al., 2016) and KlMdm12dmLys crystallized in the presence of FOS-MEA-10 (right). The domain-swapped regions are shown by black squares. **(D)** The indicated proteins were purified from *E. coli* cells and subjected to gel-filtration analyses using a HiLoad26/600 Superdex 200 pg column. Absorption at 280 nm is plotted against elution volume, and positions of molecular mass (kilodalton) marker proteins are indicated. Apparent molecular masses of the Mdm12 derivatives estimated from the peak tops (indicated with arrowheads) of the elution profiles (gel filtration) and calculated molecular masses for the monomeric derivatives (calculated) are shown in the right table. H-TEV–ScMdm12, ScMdm12 with the N-terminally attached His_{10} tag followed by the TEV protease recognition sequence; H-thrombin-KlMdm12, KlMdm12 with the N-terminally attached His_6 tag followed by the thrombin protease recognition sequence; H-thrombin–ScMdm12, ScMdm12 with the N-terminally attached His_6 tag followed by the thrombin protease recognition sequence; KlMdm12TEV-H, KlMdm12 followed by the TEV protease recognition sequence and the C-terminally attached His_6 tag; ScMdm12TEV-H, ScMdm12 followed by the TEV protease recognition sequence and the C-terminally attached His_6 tag.

folding was not affected by removal of the bound lipid (Fig. S4 E). The size and opening of the lipid-binding pocket in lipid-free KlMdm12 did not differ significantly from those of the pocket in lipid-bound KlMdm12.

Oligomeric structures of KlMdm12 and ScMdm12

The N-terminal 10 residues of Mdm12 are well conserved among different organisms (Fig. S1 A), and the ScMdm12 mutant lacking the N-terminal 11 residues caused growth defects of *S. cerevisiae* cells (Fig. 1 A), suggesting that the N-terminal segment has an important role in Mdm12 function. Jeong et al. (2016) found that purified ScMdm12 forms a homodimer, yet ScMdm12 with the N-terminally attached His_6 tag or ScMdm12 lacking the N-terminal seven-residue segment dissociates into a monomer. Furthermore, the x-ray structure of ScMdm12 showed a homodimer with domain swapping of the N-terminal seven-residue β-strand (Figs. 1 C and S1 A).

We analyzed the oligomeric states of ScMdm12 and KlMdm12 derivatives by gel-filtration chromatography (Fig. 1 D). Unexpectedly, not only the presence of the His_6 or His_{10} tag at the N or C terminus of ScMdm12 but also the following protease cleavage site sequences affected the monomer–dimer equilibrium, which is not consistent with the observations of Jeong et al. (2016). On the other hand, KlMdm12 behaved as a monomer irrespective of the position of the attached His_6 tag. Lipid-bound KlMdm12 derivatives did not form a domain-swapping dimer like lipid-bound ScMdm12, although two Mdm12 molecules are packed in a head-to-head arrangement in the crystal asymmetrical units (Fig. 1 C). FOS-MEA-10–treated lipid-free KlMdm12 formed an interlocking dimer with domain swapping of the N-terminal β-strand, which is similar to the case of lipid-bound ScMdm12 (Fig. 1 C), but this could be caused by crystal artifact. To assess the contribution of the Mdm12 interlocking dimer to its functions in vivo, we analyzed the effects of the I5P mutation in ScMdm12 on yeast cell growth (Fig. 1 A); the I5P mutation was previously shown to disrupt the N-terminal β-strand and convert the Mdm12 dimer to a monomer (Jeong et al., 2016). In contrast to the Mdm12 mutant lacking the conserved N-terminal 11 residues, Mdm12 with the I5P mutation allowed cells to grow as fast as wild-type Mdm12. Replacement of Pro5 with Ala, Asn, or Trp did not cause defects in yeast cell growth (Fig. 1 A). These results suggest that interlocking dimer formation is not essential for the functions of ScMdm12 in vivo and is therefore not an essential structural requirement for both ScMdm12 and KlMdm12.

Although ScMdm12 alone could be expressed efficiently in *E. coli* cells, KlMdm12 could be expressed to a sufficient protein level in soluble forms in *E. coli* cells only upon coexpression of residues 179–434 of *K. lactis* Mmm1 (simply referred to Mmm1s), which lacks the N-terminal residues constituting the ER luminal domain followed by the transmembrane (TM) segment. Upon coexpression with Mmm1s, the N-terminally His_6 tag–attached Mdm12 (HMdm12) was distributed as both a large hetero-oligomeric complex with Mmm1s (Mmm1s–HMdm12) and a monomeric (free) form without Mmm1s (Fig. 2 A, left). When the His_6 tag was N-terminally attached to Mmm1s (HMmm1s), Mdm12 was not dissociated from the smaller HMmm1s–Mdm12 complex (HMmm1s–Mdm12, likely $[KlMdm12]_2$–$[Mmm1s]_2$; Fig. 2 A, right) as compared with the Mmm1s–HMdm12 complex. These results suggest that KlMdm12 tends to form a hetero-oligomer with Mmm1s rather than a homodimer. We used a smaller HMmm1s–Mdm12 complex for subsequent lipid transfer assays.

Table 1. **Data collection and refinement statistics**

	Mdm12dmLys		Nonmodified Mdm12		
		+FOS-MEA10	Native	SeMet	Full-length (Mdm12FL)
Space group	P1	P321	P6122	P6122	P6122
Unit cell parameters a, b, c (Å)	42.87, 48.52, 130.13	93.39, 93.39, 81.13	136.90, 136.90, 76.56	137.17, 137.17, 76.62	137.17, 137.17, 76.62
a, b, g (°)	90.01, 91.50, 90.01	90.00, 90.00, 120.00	90.00, 90.00, 120.00	90.00, 90.00, 120.00	90.00, 90.00, 120.00
Wavelength (Å)	1	1	1	0.979	1
Resolution range (Å)	50-2.25	50-3.31	50-3.10	50-3.40	50-3.50
Number of observed reflections	527,803	535,031	1,608,644	977,533	235,394
Redundancy[a]	3.8 (3.4)	10.7 (10.7)	39.9 (39.3)	13.7 (17.7)	40.9 (43.0)
R_{merge} (%)[a]	12.3 (54.9)	10.0 (85.5)	9.1 (67.5)	13.7 (64.9)	23.6 (73.6)
I/s(I)[a]	11.3 (8.6)	15.6 (10.3)	16.6 (10.7)	13.9 (10.1)	15.0 (11.2)
Completeness (%)[a]	97.1 (87.3)	99.6 (98.8)	99.8 (99.8)	99.8 (99.8)	99.8 (100)
Refinement statistics					
Resolution range (Å)	130.08–2.25	81.13–3.31	118.56–3.10	—	39.7–3.50
Number of working sets/test sets reflections	45,717/2,438	6,065/295	7,709/371	—	5,467/260
Completeness (%)	97.1	99.6	99.8	—	99.8
R_{work} (%)/R_{free} (%)	25.1/28.6	29.6/33.5	25.3/30.7	—	26.0/32.3
Root-mean-square deviations				—	
Bond length (Å)/bond angles (°)	0.008/1.5	0.007/1.32	0.011/1.6	—	0.007/1.3
Ramachandran analysis (%)				—	
Favored	95.7	91.3	90.3	—	89.9
Allowed	100	100	100	—	100
Disallowed	0	0	0	—	0
Protein Data Bank accession no.	5H5A	5H5C	5H54	—	5H55

[a]Values in parentheses are for the highest-resolution shell only.

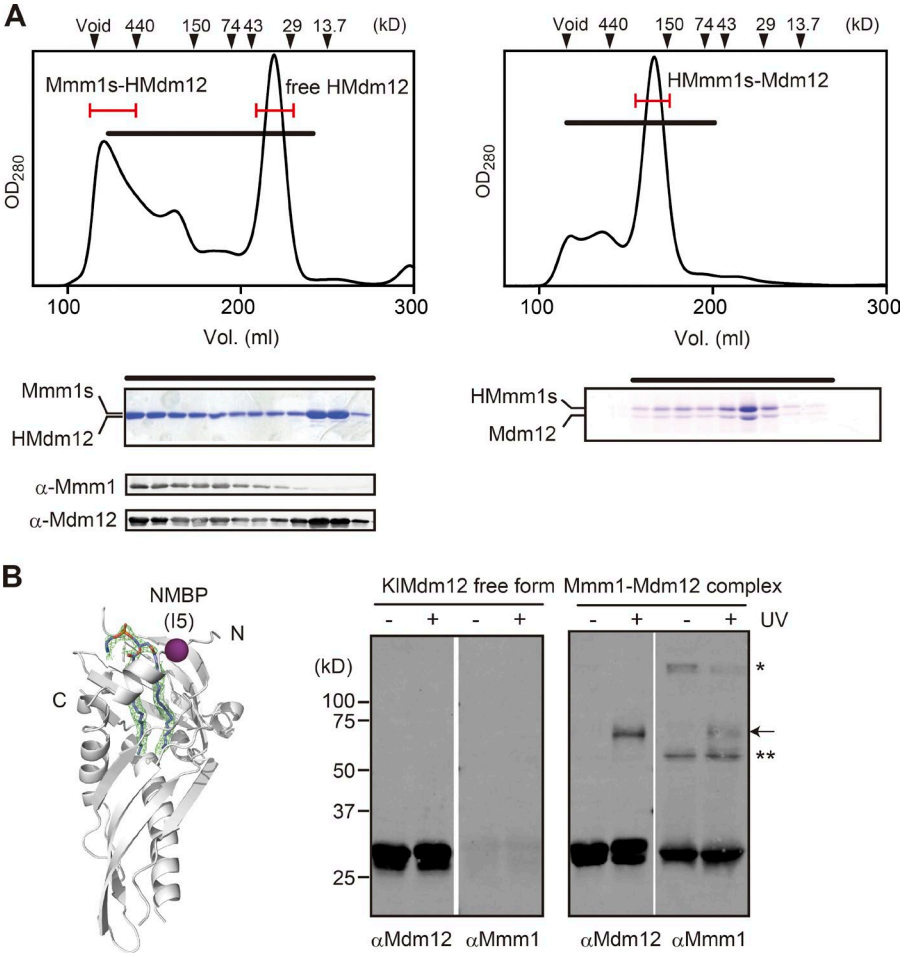

Figure 2. **Hetero-oligomer formation of *K. lactis* Mdm12 and Mmm1. (A)** KlMdm12 and Mmm1s form hetero-oligomeric complexes when expressed in *E. coli* cells. Mmm1s and N-terminally His_6-tagged KlMdm12 (HMdm12) and N-terminally His_6-tagged *K. lactis* Mmm1s (HMmm1s) and KlMdm12 were expressed in *E. coli* cells and affinity purified using a Ni-NTA column. Eluted fractions were then pooled and subjected to gel filtration by a Superdex 200 column (left: Mmm1s-HMdm12; right: HMmm1s-Mdm12). Fractions indicated with black bars in the elution profiles (top) were fractionated and analyzed by SDS-PAGE and Coomassie staining (bottom) or immunoblotting with the indicated antibodies. Fractions indicated with red bars are collected for further analyses for lipid transfer. Positions of molecular mass (kilodalton) marker proteins are indicated. The presence of the His_6 tag at the N terminus of either Mmm1 or Mdm12 affects the gel-filtration elution profiles of the Mmm1s–Mdm12 hetero-oligomers. Apparent sizes of the HMmm1s–Mdm12 and Mmm1s–HMdm12 complexes are ∼200 kD and ∼500–600 kD, respectively. **(B)** Left: The position of I5 in KlMdm12 is shown. Two forms (free KlMdm12 and KlMdm12 complexed with Mmm1s) of I5C mutant KlMdm12 were purified and modified with NMBP to introduce a photoreactive benzophenone group into the sulfhydryl group of C5. Samples were then treated with or without UV irradiation. Proteins were analyzed by SDS-PAGE followed by immunoblotting with the indicated antibodies. The arrow points to cross-linked product; asterisks indicate nonspecific signals.

To gain more insight into the oligomer formation of KlMdm12, we probed the topological arrangement of Mdm12 in the Mmm1s–Mdm12 complex by site-specific cross-linking. KlMdm12 contains three Cys (C133, C135, and C150), which are all buried or only slightly exposed to the solvent in the x-ray structure. We thus introduced additional Cys at position 5 near the entrance of the hydrophobic pocket of KlMdm12 (Fig. 2 B). We isolated both a free and Mmm1s-complexed forms of KlMdm12-I5C and labeled the Cys sulfhydryl group with a photoreactive benzophenone group. Subsequent UV irradiation led to generation of a cross-linked product, which was detected by both antibodies against Mdm12 and Mmm1, whereas KlMdm12-I5C alone or wild-type KlMdm12 in the Mmm1s–KlMdm12 complex did not generate a cross-linked product (Fig. 2 B). Therefore, the entrance of the hydrophobic pocket of KlMdm12 faces Mmm1s in the Mmm1s–Mdm12 complex, which is consistent with the low-resolution EM structure of the heterotetramer of Mmm1 and Mdm12 (AhYoung et al., 2015).

The KlMdm12 does not contain continuous tunnel for lipid binding

Three ERMES core subunits (Mdm12, Mmm1, and Mdm34) have an SMP domain, which is likely capable of lipid binding (Kopec et al., 2010, 2011). Indeed, the overall backbone structures of KlMdm12 and ScMdm12 resemble that of the SMP domain of a human extended synaptotagmin 2 (E-SYT2), which functions at the ER and plasma membrane appositions, including the presence of hydrophobic cavities and bound PE (Schauder et al., 2014). An interesting structural feature of the E-SYT2 dimer is that it has a hydrophobic continuous tunnel running through the cylinder-like dimer and accommodates two lipid-like molecules per monomer, although the continuous tunnel is still too short to bridge two membranes for lipid transport (Schauder et al., 2014; Fig. 3, A and B). In contrast, ScMdm12 and KlMdm12 have a noncontinuous hydrophobic pocket instead of a continuous tunnel, which accepts only acyl chains of one phospholipid molecule (Fig. 3, A and B). To test the possibility that the lipid-binding pocket of KlMdm12 could transiently form a tunnel or conduit running through the molecule for possible lipid transfer, we performed molecular dynamics (MD) simulation of the KlMdm12 molecule. The simulation results show that the distances between the terminal methyl atoms of the bound PE acyl chains and the hydrophobic side-chain atoms at the bottom of the lipid-binding pocket do not significantly change during 120 ns (Fig. 3, C and D). This indicates that the bottom of the lipid-binding pocket of KlMdm12 is tightly closed and is unlikely to form a continuous conduit like E-SYT2.

The Mmm1s-Mdm12 complex can transfer lipids between membranes

The present study and other biochemical as well as structural analyses (AhYoung et al., 2015; Jeong et al., 2016) showed that Mdm12 is a phospholipid-binding protein with little or moderate substrate specificities. However, it has not been demonstrated that Mdm12 has the ability to transfer lipids between

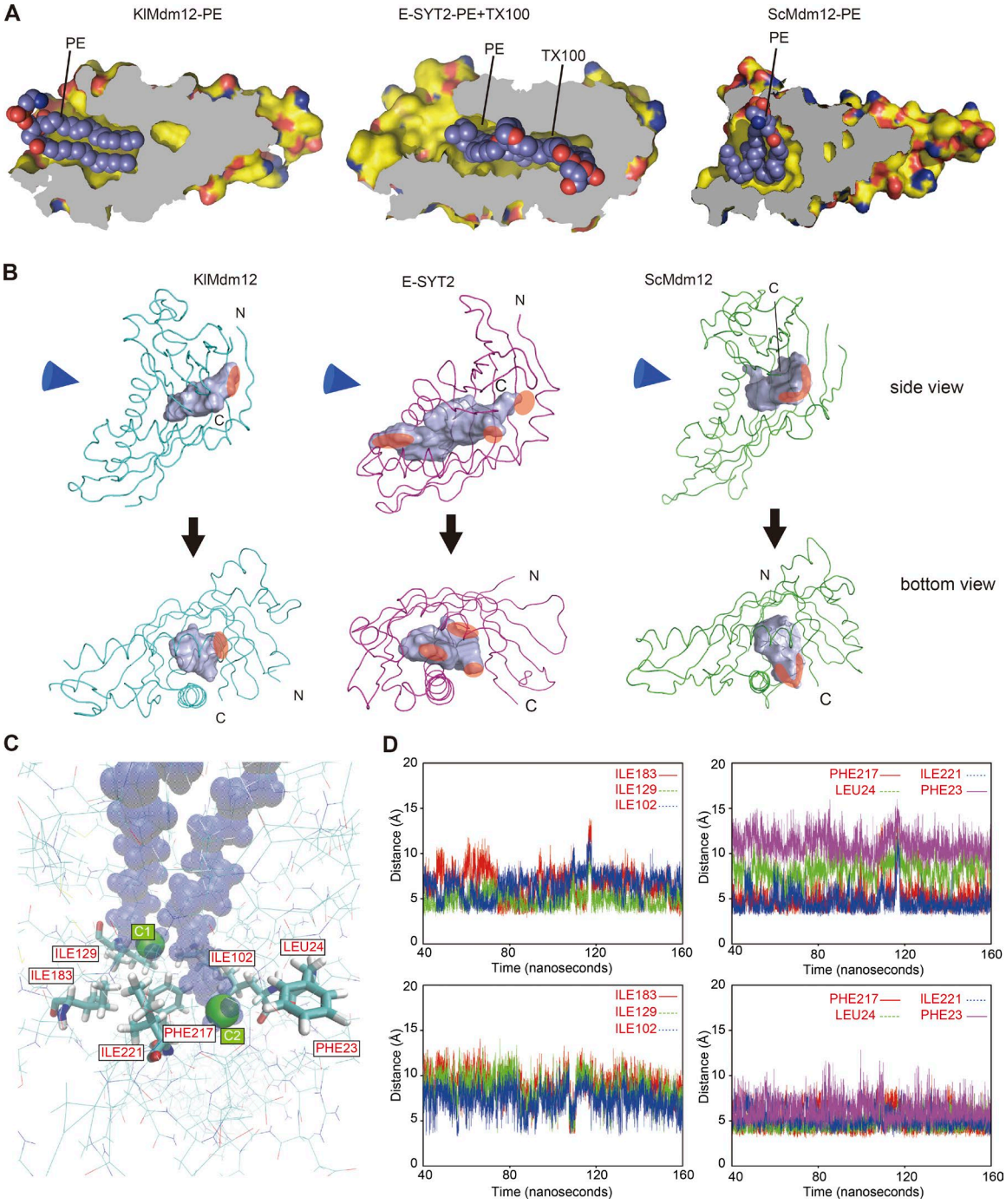

Figure 3. **Bottom of the hydrophobic pocket in KlMdm12 is tightly closed. (A)** Structural comparison of the KlMdm12–PE complex (left), the complex of E-SYT2 with PE and Triton X-100 (TX100; middle), and the ScMdm12–PE complex (right). Proteins are represented by the molecular surface (C, yellow; O, red; and N, blue) with cutaway views to show cavities and the bound substrates in space-filling form. **(B)** Solvent-accessible pockets (light blue surface) and main-chain foldings of KlMdm12 (left), human E-SYT2 (middle), and ScMdm12 (right). The solvent-accessible pockets were searched by query in the POCASSA server (http://altair.sci.hokudai.ac.jp/g6.service/pocassa/; Yu et al., 2010) and visualized. Pockets were defined as the region between the protein surface and the "probe surface," which is generated by a probe sphere with diameter of 4 Å rolling along the protein surface. Blue cones indicate the directions of the views for the bottom panels. Openings of the pockets are indicated by transparent red areas. Note that the cavity in E-SYT2 has multiple separate openings that make up a continuing cavity through the molecule. The volumes of the cavities are 1,242 Å^3, 2,086 Å^3, and 2,152 Å^3 for KlMdm12, E-SYT2 (monomer), and ScMdm12, respectively. N and C indicate the N and C termini, respectively. **(C and D)** MD simulation of the PE-bound KlMdm12 structure. MD simulation was used to test whether the bottom of the lipid-binding pocket is stably closed. The distances from the terminal methyl C atoms of the 1-palmitoyl group (C1) and of 2-oleoyl group (C2) to the hydrophobic side chains of the indicated residues (C) at the bottom of the lipid-binding pocket of KlMdm12 were traced down for 160 ns in the top and bottom panels, respectively (D).

membranes efficiently. To address this essential point, we dissected the process of lipid transfer between membranes and tested the ability of KlMdm12 to mediate each step of lipid transfer in vitro. First, we analyzed the step of lipid extraction from membranes. We thus incubated a free (monomeric) form of KlMdm12 with donor liposomes containing fluorescent

nitrobenzoxadiazole (NBD)-labeled PE and then separated proteins from liposomes by flotation with step-gradient centrifugation (Fig. 4 A). Free KlMdm12 caused only a minute shift of NBD fluorescence from floated liposome fractions to protein fractions (Fig. 4 B). Because free Mmm1s is not stable in solution, we used the fusion protein between MBP followed by HMmm1s (MBP-HMmm1s). MBP-HMmm1s caused only a marginal shift of NBD fluorescence from liposome fractions to protein fractions (Fig. 4 B). Because KlMdm12 formed a hetero-oligomeric complex with Mmm1s, we incubated the purified HMmm1s–Mdm12 complex with NBD-PE–containing liposomes as well. Surprisingly, the HMmm1s–Mdm12 complex caused a significantly enhanced shift of NBD fluorescence (Fig. 4 B). To gain information on the substrate lipid specificity of lipid extraction by HMmm1s–Mdm12, we analyzed competition by the liposomes with different phospholipid compositions in these NBD-PE extraction assays. Extraction of NBD-PE from liposomes was competed by addition of liposomes containing PC alone, PC + PE (PC/PE = 50/50), PC + PA (PC/PA = 50/50), or PC+PS (PC/PS = 50/50; Fig. 4 C). Competition was the least effective for PC-only liposomes.

As a second step of lipid transfer between membranes, we analyzed the lipid insertion from the proteins bearing a substrate lipid into membranes. We thus preloaded either free KlMdm12 or the HMmm1s–Mdm12 complex with NBD-PE and subsequently mixed them with liposomes without NBD-PE (Fig. 4 D). NBD-PE prebound to free KlMdm12 was transferred to liposomes, yet this transfer of NBD-PE was again significantly enhanced when the HMmm1s–Mdm12 complex was used instead of free Mdm12 (Fig. 4 E).

Because the lipid extraction and lipid insertion assays described in Fig. 4 do not allow evaluation of the kinetics of lipid transfer between membranes, we performed a fluorescent-based lipid transfer kinetics assay between membranes, which is similar to the PA or PS transport assay reported previously (Connerth et al., 2012; Watanabe et al., 2015; Miyata et al., 2016). Donor liposomes containing both NBD-PE and fluorescent rhodamine (Rhod)–labeled PE were incubated with free KlMdm12 or the HMmm1s–Mdm12 complex and acceptor liposomes without fluorescent lipids (Fig. 5 A). When NBD-PE is on the same liposome as Rhod-PE, NBD fluorescence is quenched by rhodamine. If free KlMdm12 or HMmm1s–Mdm12 transports NBD-PE from donor liposomes to acceptor liposomes, the fluorescence of NBD-PE will be dequenched and increase in intensity. As shown in Fig. 5 B, HMmm1s–Mdm12 increased the NBD-fluorescence of NBD-PE in a time-dependent manner, indicating that HMmm1s–Mdm12 has a phospholipid transport activity. Lipid-free, FOS-MEA-10–treated HMmm1s–Mdm12 showed a comparable lipid transfer activity. On the other hand, the free form of Mdm12 or the MBP-HMmm1s fusion protein showed only marginal lipid transfer activities. Next, we compared the transfer of NBD-PE with that of PS labeled with NBD (NBD-PS) between liposomes (Fig. 5, C and D). Efficiency of NBD-PS transfer between liposomes by HMmm1s–Mdm12 was threefold higher than that of NBD-PE transfer, although the structural basis of this difference in lipid transfer efficiency is not clear. Therefore, although free Mdm12 and Mmm1s like the MBP-HMmm1s fusion protein are capable of transferring phospholipid between liposomes inefficiently, the lipid-transfer activity of Mmm1s and/or Mdm12 becomes significantly higher when they form a complex.

We then tested the effects of mutations in Mmm1 on the lipid transfer activities of HMmm1s–Mdm12 and MBP-HMmm1s (Fig. 5 E). On the basis of the predicted homology model of Mmm1s, we introduced mutations (V190S, L274S, or I369S) in the putative hydrophobic pocket in Mmm1s (Fig. 5 G). I369S and L274S, but not V190S, mutations partially suppressed the lipid transfer activity of free MBP-HMmm1s and the HMmm1s–Mdm12 complex. We also tested the effects of similar mutations in Mdm12 on the lipid transfer activities of the Mmm1–Mdm12 complex (Fig. 5 F). However, because KlMdm12 mutants tend to destabilize the oligomeric structures of HMmm1s–Mdm12, we analyzed lipid transfer by the complex of ScHMmm1s and ScMdm12 instead of the *K. lactis* HMmm1s–Mdm12 complex. We prepared ScMdm12, L10S, V125S, V214S, and E255R in the hydrophobic pocket (Fig. 5 G); L10, V125, and V214 in Mdm12 correspond to the positions of V190, L274, and I369, respectively, in Mmm1, and E255R in ScMdm12 was previously shown to exhibit weaker PC binding activity than wild-type ScMdm12 (Jeong et al., 2016). Although ScHMmm1s–Mdm12 variants showed much lower lipid transfer activity than KlHMmm1s–Mdm12 (Fig. 5, E and F), all the mutations in ScMdm12, including L10S corresponding to V190S in Mmm1, lowered the lipid transfer activity of the Mmm1–Mdm12 complex. It should be noted that the N-terminal 11 residues, including L10 in Mdm12, are essential for Mdm12 functions in vivo (Fig. 1 A). These results indicate that both Mmm1s and Mdm12 are responsible for the high lipid transfer activity of the Mmm1–Mdm12 complex.

Mmm1 mediates PS transfer from the ER to mitochondria via ERMES

Finally, we asked whether the Mmm1 mutations (V190S, L274S, or I369S in *K. lactis* Mmm1s) and ScMdm12 mutations (L10S, V125S, V214S, or E255R) that mostly affect lipid transfer between liposomes to a different extent in vitro could also affect lipid transport between the ER and mitochondria via ERMES. For this purpose, we used the recently developed in vitro assay system with the isolated yeast heavy-membrane fraction (HMF) to monitor the phospholipid exchange between the ER and mitochondria directly (Kojima et al., 2016). In brief, incubation of radioactive [^{14}C]-serine with the HMF containing mitochondria and the ER membrane allows formation of radiolabeled PS in the ER. Radiolabeled PS is transported from the ER to mitochondria for conversion to PE, which is then transported from mitochondria to the ER for conversion to PC via the intermediate phosphatidyldimethylethanolamine (Fig. 6 A).

We isolated HMF from *mmm1*Δ cells expressing Vps13-D716H and wild-type or mutant *S. cerevisiae* Mmm1 (V190S, L274S, L274S/L369S, or L369S) and from *mdm12*Δ cells expressing wild-type or mutant *S. cerevisiae* Mdm12 (L10S, V125S, V214S, or E255R). Expression of Vps13-D716H was reported to suppress the growth defects in ERMES-lacking cells (Lang et al., 2015). The protein levels of Mmm1 and Mdm12 derivatives, phospholipid synthetic enzymes (e.g., Cho1, Psd1, Cho2, and Opi3), and a control protein (Tim23) did not differ significantly among HMFs isolated from those strains (Fig. S5 A). We then incubated the HMFs with [^{14}C]-serine for different periods of time and analyzed synthesized phospholipids by TLC followed by radioimaging. Radioactive phospholipids were quantified, and the amounts of each phospholipid to total radioactive phospholipids or PE were plotted against the incubation time (Fig. S5, B and C). The relative amounts of

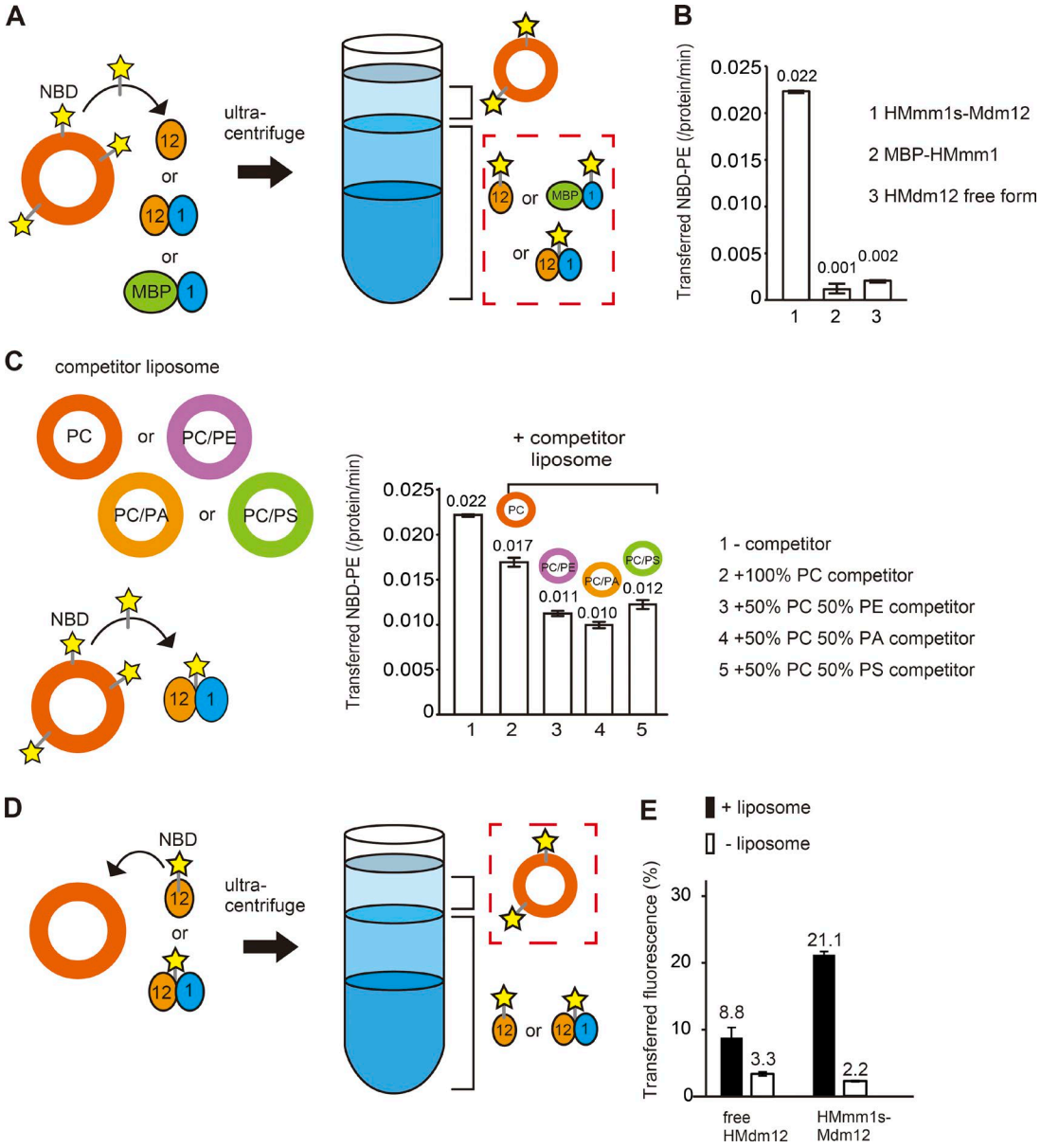

Figure 4. **Mmm1–Mdm12 can extract lipids from membranes and insert them into membranes. (A)** Fluorescent lipid extraction by a protein from liposomes. Liposomes consisting of PC and NBD-PE (PC/NBD-PE = 80/20) were incubated with free KlMdm12, MBP–HMmm1s, or HMmm1s–Mdm12 and then separated by sucrose step-gradient centrifugation. The orange and blue ovals indicate Mdm12 and Mmm1s, respectively. **(B)** Lipid-extraction activities as fluorescence intensity in the protein fraction in the assay in A (broken-line square) are plotted by bars and figures above the bar. Bars show means ± SE of three independent experiments. **(C)** Competition of HMmm1s–Mdm12–mediated fluorescent lipid extraction from liposome by nonfluorescent liposomes. 200 µM liposomes (PC/NBD-PE = 80/20) were incubated with HMmm1s–Mdm12 in the presence or absence of 200 µM PC liposomes (orange), PC/PE (50/50; purple), PC/PA (50/50; yellow orange), or PC/PS (50/50; yellow green) liposomes and separated by sucrose step-gradient centrifugation. The molar ratio of transferred NBD-PE to HMmm1s–Mdm12 was plotted by bars and figures above the bars. Bars show means ± SE of three independent experiments. Total NBD-PE fluorescence intensity was estimated by solubilizing NBD-PE–containing liposomes with Triton X-100. **(D)** Lipid transfer from a protein preloaded with a fluorescent lipid to liposomes. Free form of Mdm12 (free Mdm12) or HMmm1s–Mdm12 preloaded with NBD-PE was incubated with PC liposomes and then separated by Nycodenz step-gradient centrifugation. **(E)** Lipid-transfer activities (protein to liposomes) as fluorescence intensity in the floating liposome fraction normalized by the fluorescence intensity in total fractions are plotted by bars and figures above the bars. Bars show means ± SE of three independent experiments. We confirmed that the added proteins did not stably bind to liposomes in these assays.

PS to total phospholipids (PS/total) efficiently decreased in a time-dependent manner in wild-type membrane fractions, whereas PS synthesis, which was reflected in the total phospholipids (total), lasted for 30 min of incubation (Fig. S5, B and C, WT, PS/total, and total). This decrease in PS/total reflects the PS transport from the ER to mitochondria. Notably, the loss or mutations (V190S, L274S, L369S, and L274S/L369S) of Mmm1 decreased PS transport rates compared with that of the wild-type membrane fractions (Fig. 6 B). The loss of mutations (L10S, V125S, and V214S), but not mutation E255R, of Mdm12 also decreased the PS transport rates compared with that of the wild-type membrane fractions (Fig. 6 C). These results indicate that phospholipid transfer between liposomes by the isolated Mmm1s–Mdm12 complex observed in vitro (Fig. 4) may reflect the lipid transport by ERMES between mitochondria and the ER.

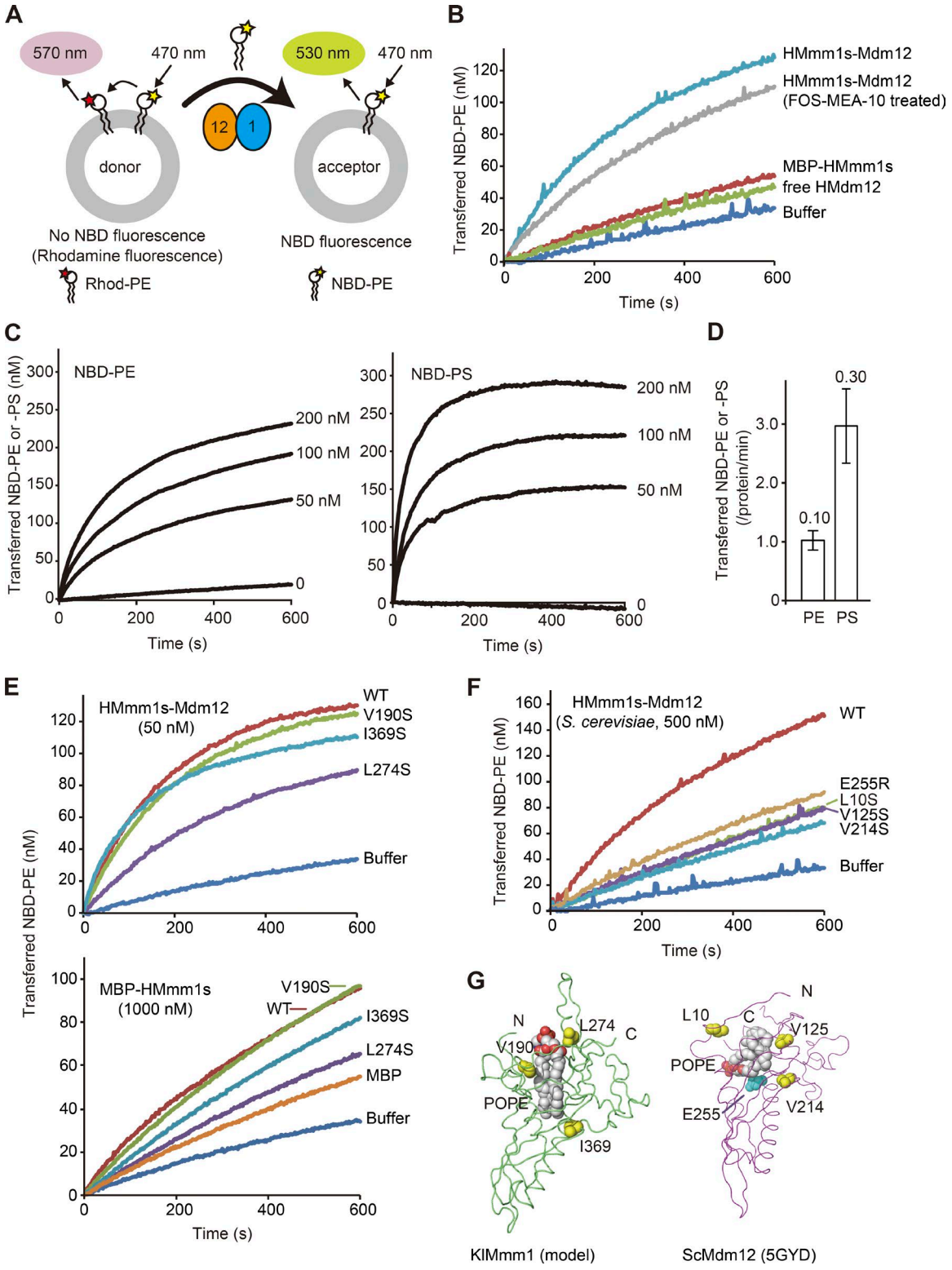

Figure 5. **Mmm1–Mdm12 can transfer lipids between lipid membranes. (A)** A schematic diagram of the fluorescent-based NBD-PE transfer between liposomes. 12.5 µM donor liposomes contain NBD-PE and Rhod-PE, and NBD fluorescence is quenched by FRET to Rhod. Once NBD-PE is transferred to acceptor liposomes (50 µM), NBD fluorescence increases, which is monitored in B. **(B)** NBD-PE transfer activities of the 50 nM HMmm1s–Mdm12 complex, the FOS-MEA-10–treated HMmm1s–Mdm12 complex, MBP-HMmm1s, and HMdm12 were measured at 25°C by the assay shown in A. At 0 s, the protein or buffer was added to the reaction mixture, and NBD fluorescence intensities were set to 0 at 0 s. **(C)** Transfer of NBD-PE and NBD-PS between liposomes by different concentrations of HMmm1s–Mdm12 was compared by the assays as in B. **(D)** The amounts of NBD-PE and NBD-PS transferred from 12.5 µM donor liposomes containing NBD-PE or NBD-PS with Rhod-PE to 50 µM acceptor liposomes after 10 s reaction. Total NBD-PE or NBD-PS fluorescence intensities were estimated by solubilizing NBD-PE or NBD-PS containing liposomes with Triton X-100. Bars show means ± SD of three independent experiments. **(E)** NBD-PE transfer activities of the 50 nM HMmm1s–Mdm12 complex and 1,000 nM MBP-HMmm1s containing *K. lactis* wild-type Mmm1s (WT) or the indicated *K. lactis* Mmm1s mutants (measured as in A and B). Total NBD-PE fluorescence intensity was estimated by solubilizing NBD-PE–containing

Discussion

A fundamental question concerning ERMES in yeast is whether it is directly involved in lipid trafficking between the ER and mitochondria, and if so, how hydrophobic lipid molecules can be transported between the organelles by crossing the aqueous cytosol. Here, we focused on *K. lactis* Mdm12 and Mmm1, the peripheral membrane protein subunit and the ER-anchored subunit of ERMES, respectively, and analyzed their roles in lipid transfer between membranes. We first determined the x-ray structures of KlMdm12 with and without bound phospholipid and compared them with that of ScMdm12 complexed with phospholipid. KlMdm12 and ScMdm12 have a similar hydrophobic pocket in the cone-shaped molecules into which phospholipid can bind. Mutational analyses, including that of the Mdm12 I5P mutant, showed that the head-to-head homodimer formation of Mdm12 observed for the ScMdm12 x-ray structure (Jeong et al., 2016) is not necessary for the function of Mdm12 in vivo.

The structures of ScMdm12 and KlMdm12 and identification of phospholipids in their hydrophobic cavities clearly established that Mdm12 is a lipid-binding protein. However, when tested in vitro, purified free KlMdm12 alone or Mmm1s as a purified fusion protein (MBP-HMmm1s) is capable of extracting phospholipid from donor liposomes and transferring it to acceptor liposomes, but this lipid transfer activity is very low. On the other hand, the ability to transfer lipids is significantly enhanced when KlMdm12 and Mmm1s form a hetero-oligomeric complex with each other. The lipid transfer activity of the Mmm1s–Mdm12 complex is impaired by mutations in both Mmm1s and Mdm12. Furthermore, these Mmm1 and Mdm12 mutations also impaired ERMES-dependent PS transport from the ER to mitochondria in the in vitro lipid transport assays with isolated mitochondria and the ER membranes. This indicates that the lipid transfer activity of the Mmm1s–Mdm12 complex between membranes arises from the cooperation of Mmm1s and Mdm12.

How does the Mmm1–Mdm12 complex mediate phospholipid transfer between membranes? An attractive model is that Mmm1 has the ability to extract lipids from and insert lipids into the ER membrane and thereby functions as an extractor or inserter of lipids in the ER membrane. For lipid transport from the ER to the mitochondrial OMs, Mmm1 should pass the extracted lipid over to Mdm34 via Mdm12. The revealed geometry of the entrance of the lipid-binding pocket of Mdm12 in contact with Mmm1 supports this idea. For the transfer of the lipid from Mmm1 to Mdm12, two possible models can be considered (Fig. 7). In the lipid carrier model (Fig. 7 A), Mmm1 may change the relative geometry to Mdm12 from the tail (Mmm1)-to-head (Mdm12) contact to the head (Mmm1)-to-head (Mdm12) contact, so that the phospholipid molecule bound to the hydrophobic pocket of Mmm1 can be transferred to the one of Mdm12 through the outlets of the both pockets at the head-to-head interface between Mmm1 and Mdm12. Upon receiving the phospholipid molecule from Mmm1, Mdm12 may switch the partner from Mmm1 to Mdm34, with changing the relative geometry to Mdm34 from the tail (Mdm12)-to-head (Mdm34) to the head (Mdm12)-to-head (Mdm34) contact for further lipid transfer. Mdm34 also contains an SMP domain and may thus be another possible lipid-binding component on the mitochondrial surface like Mmm1 in the ER membrane. Therefore, a switch between the heterodimeric structural units consisting of the SMP domains of Mdm12 and Mmm1 and of Mdm12 and Mdm34, with changing relative geometry to each other, may facilitate lipid transfer between the ER and mitochondrial OMs. Another possible model for lipid transport from ER to mitochondria, the continuous conduit model (Fig. 7 B), assumes the presence of a continuous hydrophobic tunnel running all the way from Mmm1 to Mdm34 via Mdm12. The phospholipid molecule extracted by Mmm1 from the ER membrane may diffuse through the hydrophobic conduit via Mdm12 to reach Mdm34 and is then inserted into the mitochondrial OM by Mdm34. Our observation that the bottom of the hydrophobic pocket of Mdm12 is tightly closed favors the lipid carrier model, yet stable complex formation between Mmm1 and Mdm12, without any dynamic exchange of Mmm1 or Mdm12 with their free forms, favors the continuous conduit model. The question of which of these speculative models is correct should be addressed experimentally in future studies.

Materials and methods

Plasmids

The plasmids used here were constructed by standard recombinant DNA techniques. For expression of Mdm12(1–239) from *K. lactis* (KlMdm12) in *E. coli* cells, the DNA fragment for KlMdm12 was amplified from the genome of *K. lactis* and cloned into pET-21d (for nontagged Mdm12; Merck), pET-15b (for KlMdm12 with the N-terminal His_6 tag [HMdm12]), or pET-16b (for KlMdm12 with the N-terminal His_{10} tag). For expression of His-thrombin-ScMdm12, ScMdm12-TEV-His, and His-TEV-ScMdm12 in *E. coli* cells, the DNA fragments for corresponding ScMdm12 derivatives were amplified and ligated into pET-15b, pET-22b, and pRSF-1b, respectively. The plasmids for coexpression of the soluble domain of Mmm1 from *S. cerevisiae* and ScMdm12 were prepared as follows. A DNA fragment for Mmm1 from *S. cerevisiae* (184–426, ScMmm1s) was cloned into pET-15b at the NdeI and BamHI sites and amplified by PCR with a DNA fragments for the His_6 tag and thrombin cleavage sequence. The resulting DNA fragment was cloned into pRSF-1b. The expression plasmid for ScMdm12 without the His_6 tag was constructed after cloning into pET-22b using the NdeI and BamHI sites. For expression of Mmm1(179–434) from *K. lactis* (Mmm1s), the DNA fragment for Mmm1s was amplified and ligated into pET-15b (for Mmm1 with the N-terminal His_6 tag [HMmm1s]) or pACYC-Duet (for nontagged Mmm1). For expression of *S. cerevisiae*

liposomes with Triton X-100. **(F)** NBD-PE transfer activities of the 500 nM ScHMmm1s–ScMdm12 complex analyzed as in E. The curves for the mutations at the same positions between the Mmm1 model structure (E) and Mdm12 x-ray structure (F) are indicated with the same colors. **(G)** Positions of the mutated hydrophobic residues in the *S. cerevisiae* Mdm12 structure (Jeong et al., 2016) and in the homology model of *K. lactis* Mmm1s (KlMmm1s, main-chain folding in green) are shown by space-filling form in yellow. E255 in the *S. cerevisiae* structure is shown by space-filling form in cyan. The positions of POPE in the ScMdm12 structure and in the model structure of KlMmm1s are shown in space-filling form. Homology modeling of KlMmm1s based on the KlMdm12 structure was performed using Modeller software (Šali and Blundell, 1993). The predicted model structure of KlMmm1s resembles KlMdm12 and possesses a hydrophobic (likely phospholipid-binding) pocket. To assess the significance of the hydrophobic pockets of Mmm1 and Mdm12 in lipid transfer activity by mutational analyses, three residues were chosen according to their positions at the entrance, middle, and bottom part of the pocket: L10, V125, and V214 in ScMdm12 and V190, L274, and I369 (KlMmm1 numbering) in KlMmm1.

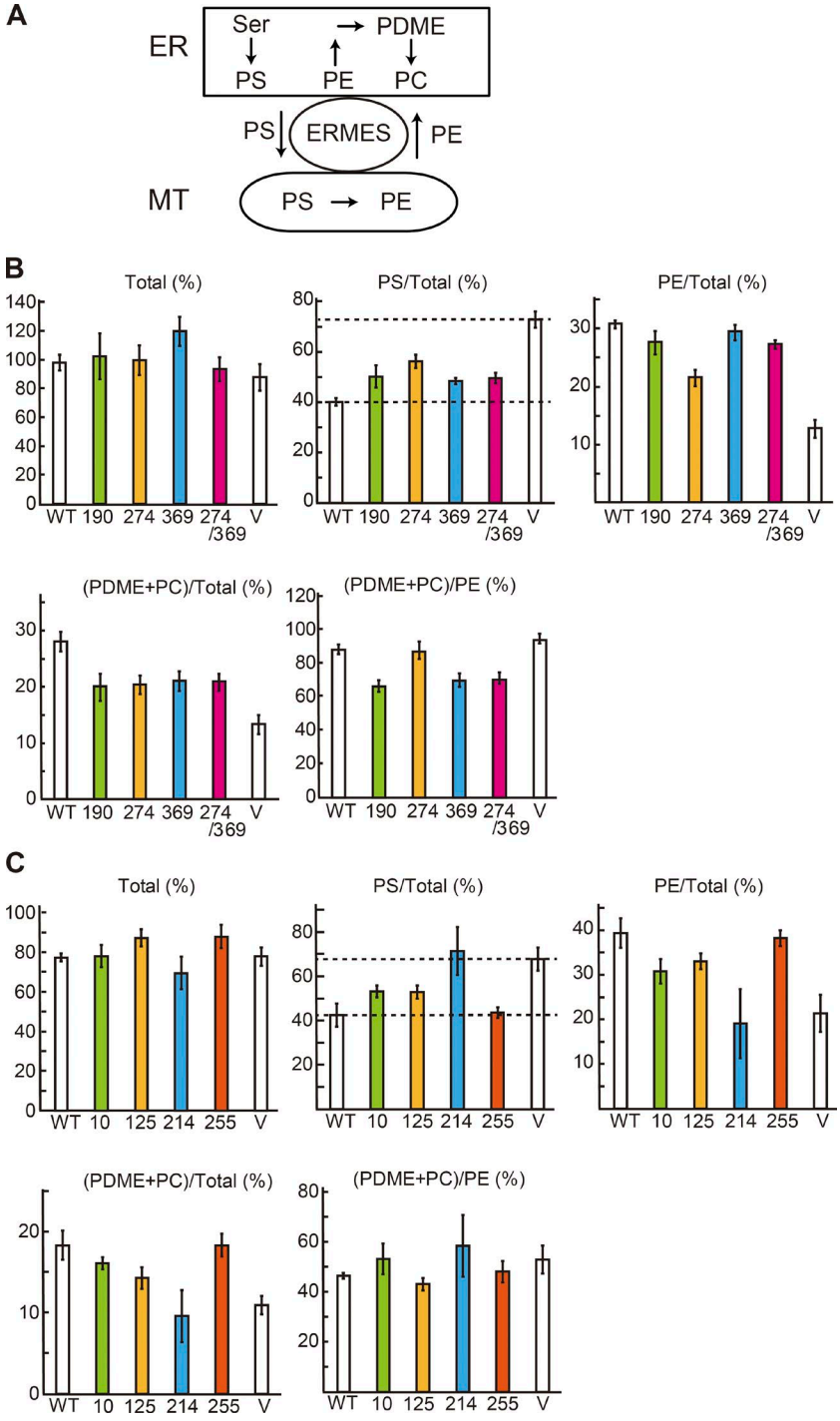

Figure 6. **Mmm1 and Mdm12 mediate PS transport from the ER to mitochondria. (A)** A schematic diagram of the PS transfer/conversion pathway involving the ER and mitochondria (MT). The indicated phospholipids were analyzed in this assay. PDME, phosphatidyldimethylethanolamine. **(B)** In vitro PS transport assays were performed using the HMFs isolated from *mmm1*Δ cells expressing Vps13-D716H with *S. cerevisiae* wild-type (WT) or mutant Mmm1 (V190S [190], L274S [274], L369S [369], or L274S/L369S [274/369]) or without Mmm1 derivatives (V). Total phospholipids were extracted and analyzed by TLC and radioimaging. Amounts of PS, PE, and PDME+PC relative to total phospholipids and PDME+PC relative to PE were quantified after 30 min of incubation. Bars show mean ± SE of three independent experiments. The amount of total phospholipids synthesized with wild-type cells after 40-min incubation was set to 100% (total). The amounts of PS/total reflect PS transport from the ER to mitochondria. **(C)** In vitro PS transport assays were performed using the HMFs isolated from *mdm12*Δ cells expressing Vps13-D716H with *S. cerevisiae* wild-type (WT) or mutant Mdm12 (L10S [10], V125S [125], V214S [214], or E255R [255]) or without Mdm12 derivatives (V) as in B. The amounts of PS/total reflect PS transport from the ER to mitochondria. The bars for the mutations at the same positions between the Mmm1 model structure (B) and Mdm12 x-ray structure (C) are indicated with the same colors.

Mdm12 (ScMdm12) for lipidome analyses, DNA for ScMdm12 was PCR amplified and cloned into pET-30a(+) (Novagen). Plasmids for expression of KlMdm12 or Mmm1 in yeast cells were prepared as follows. The *MDM12* and *MMM1* genes containing ∼500- and 300-bp regions upstream and downstream of the initiation and stop codons in the open reading frame, respectively, were PCR amplified using the *S. cerevisiae* genome DNA as template and cloned into the *TRP1*-containing pRS314 or pRS316 vector.

Yeast strains and growth conditions

The *mdm12Δ* and *mmm1*Δ strains (with expression of Vps13-D716H) were described in Tamura et al. (2012) and Kojima et al. (2016), respectively. The *mdm12Δ* strain, which lacks the chromosomal *MDM12* gene and is complemented with the *URA3* plasmid bearing the *MDM12* gene, was transformed with a *TRP1*-containing single-copy plasmid harboring the genes for Mdm12 from *S. cerevisiae* and Mdm12 mutants, including Mdm12 (1–239), from *K. lactis*. The resulting strains were cultured on SCD-Trp plates containing 5′-fluoroorotic acid to obtain strains expressing *S. cerevisiae Mdm12* and *K. lactis Mdm12* mutants. Cells were grown in SCD (0.67% yeast nitrogen base without amino acids, 0.5% casamino acid, and 2% glucose) or SCLac (0.67% yeast nitrogen base without amino acids, 0.5% casamino acid, and 2% lactate) media with appropriate supplements.

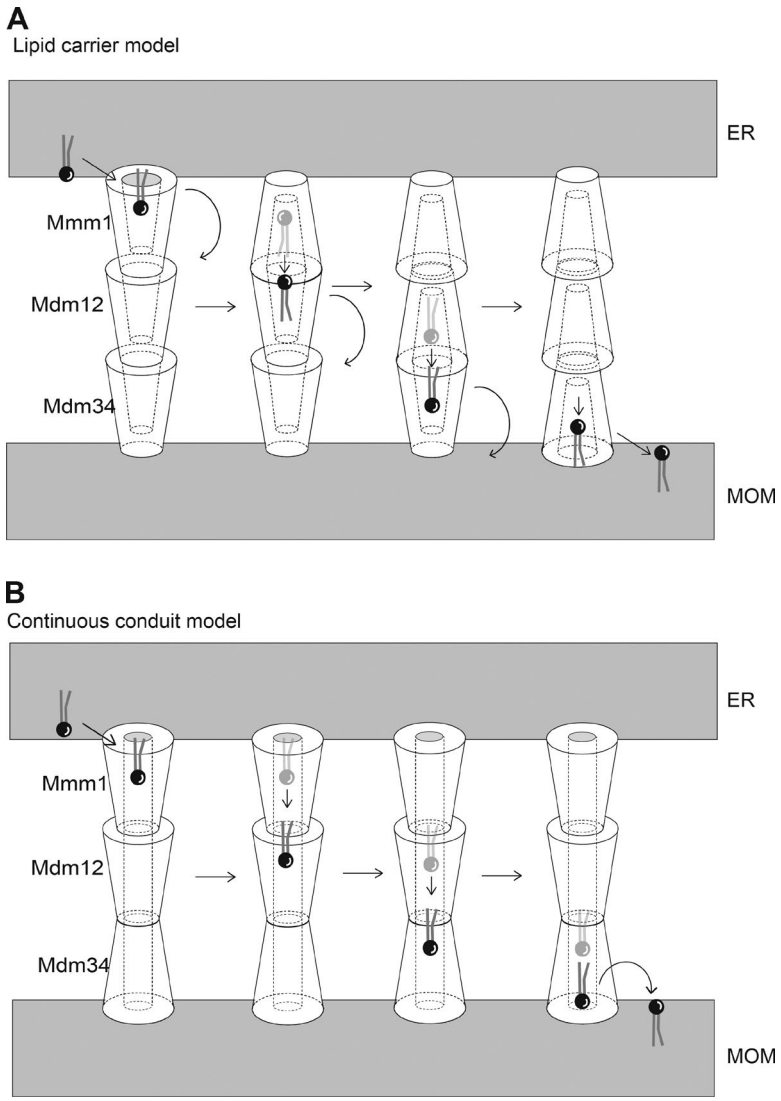

Figure 7. **Models of phospholipid transfer by ERMES between the ER and mitochondrial OMs. (A)** Lipid carrier model assumes that Mmm1, Mdm12, and Mdm34 have a hydrophobic lipid-binding pocket with an outlet only at the head of the molecules for binding to a phospholipid molecule. They pass the lipid molecule sequentially from Mmm1 at the ER membrane to Mdm34 at the mitochondrial OM via Mdm12 for the lipid transport from the ER to mitochondria. To achieve efficient transfer of lipid molecules between each ERMES component, they have to change their orientations and positions relative to the other components to put the outlet of the lipid-binding pocket of one component close to the one of the other component. **(B)** The continuous conduit model assumes the presence of the hydrophobic lipid-binding tunnels with two outlets at the head and tail of the molecules of Mmm1, Mdm12, and Mdm34. These tunnels are connected with each other to form a continuous lipid-moving conduit running from Mmm1 to Mdm34 via Mdm12. For lipid transport from the ER to mitochondria, a lipid molecule extracted from the ER membrane by Mmm1 will enter the hydrophobic tunnel in Mmm1 and diffuse through the tunnel to reach the one in Mdm12 and then the one in Mdm34. Finally, the lipid molecule will be released from the other outlet of the tunnel of Mdm34 for insertion into the mitochondrial OM.

Protein expression, purification, and modification

For crystallization, KlMdm12 (residues 1–239) and KlMdm12FL (residues 1–305) were coexpressed with *K. lactis* Mmm1s (residues 179–434) in *E. coli* strain Rosetta (DE3) or BL21(DE3) by incubation at 16°C for 16 h after addition of 0.5 mM IPTG (isopropyl-D-thiogalactoside). Free KlMdm12 or KlMdm12FL dissociated from the Mmm1s-Mdm12(FL) complex was purified by affinity chromatography for the His_6 tag attached to the N-terminus of KlMdm12(FL).

For lipidomics analysis of bound lipids for ScMdm12, the expression plasmid was transformed into BL21(DE3) +pRARE bacteria (Promega). The cells were grown in 2 l kanamycin- and chloramphenicol-containing LB medium to an OD of 0.6. The cells were then cooled down on ice, induced with 1 mM IPTG, and allowed to express the protein for 16–20 h at 15°C. The cells were then harvested by centrifugation, washed with lysis buffer (1 M NaCl, 5 mM $MgCl_2$, 50 mM Tris-HCl, pH 7.4, 30 mM imidazole, 1 mM PMSF, and 1 mM DTT), and processed for Mdm12 purification. Cell pellet was resuspended in 40 ml lysis buffer and sonicated on ice. One tenth (4 ml) of the sonicated cell suspension was kept for total cellular lipid quantification. After centrifugation, the supernatant was applied to a 5-ml HisTrap column (GE Healthcare), washed with 60 ml of lysis buffer and eluted in the same buffer containing 300 mM imidazole. The fractions containing the protein were pooled and dialyzed against the same buffer without imidazole and PMSF but containing 0.5 M NaCl. The protein was then applied to a HiPrep Superdex 200 26/60 column (GE Healthcare). The fractions containing the monomeric peak were pooled.

For preparation of KlMdm12 variants, the *E. coli* strain Rosetta (DE3) or BL21(DE3) (Merck) bearing plasmids for expression was cultured at 37°C in LB media containing ampicillin or chloramphenicol. Expression of proteins was induced by adding 0.5 mM IPTG when OD_{600} reached to 0.5, and then the cells were further incubated at 16°C for 16 h. The selenomethionine (SeMet)-labeled proteins were prepared from *E. coli* cells cultured in minimal media containing 50 mg/l SeMet. The cells were harvested, washed with 20 mM Tris-HCl, pH 7.4, and 300 mM NaCl (TBS300), and disrupted by sonication in TBS300. After centrifugation, the supernatant was loaded onto a Ni-NTA (QIAGEN) column and washed with TBS300 containing 20 mM imidazole, pH 8.0. The target proteins were eluted by TBS300 containing 500 mM imidazole, pH 8.0, and further purified by a Hiload 26/600 Superdex 200 pg column (GE Healthcare) with 20 mM Tris-HCl, pH 7.4, and 150 mM NaCl (TBS150). For high-quality crystal production, the eluted His_{10}-KlMdm12 (HMdm12) fractions were combined and treated with factor Xa protease (QIAGEN) to remove the N-terminal affinity tags. The cleaved proteins were subjected to reductive methylation of Lys and applied to a Superdex 200 10/300 GL column to obtain purified target proteins.

Reductive methylation of Lys in KlMdm12 was performed according to methods reported previously (Bokoch et al., 2010), with minor modifications. In brief, 10 ml of 1 mg/ml Mdm12 in 20 mM Hepes-NaOH, pH 7.4, and 100 mM NaCl was mixed with 500 µl of 2% (wt/vol) dimethylaminoborane and 30 µl formaldehyde and incubated for 4°C for 16 h, and then 200 µl of 2% (wt/vol) dimethylaminoborane and 20 µl formaldehyde were added for further incubation at 4°C for 4 h. The reaction was quenched by 20 mM Tris-HCl, pH 7.4, and the modified proteins were purified by gel filtration chromatography.

The plasmid for expression of the MBP-KlaMmm1s, a fusion protein of MBP followed by *K. lactis* Mmm1s (179–434) with a linker segment consisting of the TEV protease recognition sequence, His_6 tag, and thrombin recognition sequence between them was constructed as follows. The pET-15b plasmid bearing DNA for *K. lactis* Mmm1s (179–434) was used to amplify the fragment with the coding sequence for His_6 tag followed by the thrombin recognition sequence, and the resultant DNA fragment was cloned into the pMal-c2x vector (NEB). The TEV protease recognition sequence was inserted between MBP and the His_6 tag at the DNA level. MBP-KlaMmm1s was expressed and purified according to essentially the same procedure used for the Mmm1–Mdm12 complex. MBP was expressed in the same manner as other proteins and purified by amylose resin (NEB) in TBS150 containing 1 mM EDTA by using elution buffer (20 mM maltose and 1 mM EDTA in TBS150). The eluate was collected and loaded onto a Hiload 26/600 Superdex 200pg column in TBS150, and eluted MBP was pooled and concentrated. Mutagenesis of *K. lactis* Mmm1 was performed with oligonucleotide-directed PCR mutagenesis using adequate primers. Mmm1s–HMdm12 and MBP-HMmm1s containing mutant Mmm1s were expressed in *E. coli* cells and prepared by the same procedures as those containing wild-type Mmm1s.

The N-terminally His_6-tagged ScHMmm1s and ScMdm12 were coexpressed in the BL21(DE3) strain and purified as KlHMmm1s and KlMdm12 by gel filtration and ion exchange chromatography using a COSMOGEL IEX type Q column (Nacalai Tesque).

Crystallization and data collection

Purified KlMdm12 derivatives were concentrated to ∼10 mg/ml and screened with manufactured crystallization screening kits (Hampton research) using an automated robot system mosquito (TTP Labtech) by the sitting-drop vapor-diffusion method at 25°C. Successful conditions that generate crystals were refined to obtain crystals suitable for x-ray diffraction experiments using the hanging-drop vapor-diffusion method. X-ray diffraction data collection were performed for the HMdm12 crystals grown in 0.2 M malate-2Na, 0.1 M Tris-HCl, pH 8.0, and 20% polyethylene glycol 3350. The SeMet-labeled HMdm12 derivative was crystallized under the similar condition. The chemically modified KlMdm12 was crystallized in 1.4–1.6 M sodium potassium phosphate, pH 8.2, and 20% glycerol with or without 5.3 mM detergent FOS-MEA-10 (Anatrace). To remove FOS-MEA-10 from the grown crystals, the crystals were washed with Biobeads (Bio-Rad) in fresh mother liquors for twice and left in the same buffer for at least 3 wk. X-ray diffraction data collection was performed at beamline BL38B1 and BL44XU in SPring-8. The crystals were mounted on the cryo-loop (Hampton Research) and flush cooled in the liquid nitrogen stream. The data were collected up to 3.1 and 3.5 Å resolution for native and SeMet-labeled HMdm12, respectively. The chemically modified protein crystals gave diffraction up to 2.25 Å resolution, and the crystals grown in the presence of FOS-MEA-10 up to 3.3 Å resolution. The diffraction data were processed with HKL2000 (Otwinowski and Minor, 1997). The statistics of the data collection are summarized in Table 1.

Structure determination

The phase problem was solved by an automated software suite (PHENIX; Adams et al., 2010) using single-wavelength anomalous dispersion data from the crystals of SeMet-labeled HMdm12. The structure was refined by refmac5 (Murshudov et al., 2011) and CNS (Brünger et al., 1998), and manual model building was performed by Coot (Emsley et al., 2010). The optimization of secondary structures and energy minimization were performed using a 3D refine web service (Bhattacharya and Cheng, 2013). The structures of native or chemically modified proteins were solved by the molecular replacement method using the constructed model from SeMet-labeled HMdm12 as a search model by PHASER (McCoy et al., 2007) in the CCP4 suite (Collaborative Computational Project, Number 4, 1994). The determined structures were validated by Rampage (Lovell et al., 2003), and secondary structure analysis was performed by DSSP (Kabsch and Sander, 1983; Joosten et al., 2011). Structural images were drawn using PyMOL Molecular Graphics System (version 1.7.0; Schrödinger).

Atomic coordinates and structure factors files have been deposited in the Protein Data Bank under accession numbers 5H54 (KlMdm12(1–239), native), 5H55 (KlMdm12FL from *K. lactis*, full-length protein), 5H5C (KlMdm12(1–239) with dimethyl lysine modification and FOS-MEA-10 treatment), and 5H5A (KlMdm12(1–239) dmLys with dimethyl-lysine modification).

Lipid analyses

Lipids bound to free KlMdm12 were extracted as follows. The free form of KlMdm12 was purified from *E. coli* cells expressing both KlMdm12 and Mmm1s and was vigorously vortexed in 2:1 chloroform/methanol for 20 min. One-fourth volume of 0.1M HCl and 0.1 M KCl was then added, and the sample was further vortexed for 10 min. The organic phase separated by a low-speed spin was dried under a nitrogen stream and subjected to TLC analysis.

ScMdm12-bound lipids as well as total lipids were extracted from *E. coli* cells, without coexpression of Mmm1, using the Folch procedure (Folch et al., 1957). Lipidomic analysis was performed as described previously (Guan et al., 2010) on a TSQ Vantage triple quadrupole mass spectrometer (Thermo Fisher Scientific). Quantifications of relative amounts of lipids were performed by calculating the area under the curve in the full-scan mass spectrogram for each lipid species analyzed.

Preparation of proteins preloaded with NBD-PE

Chemical modification of the amino group of phospholipids with 4-fluoro-7-nitrobenzofurazan (NBD-F; Dojindo) was performed according to the manufacturer's protocol. *E. coli* total phospholipids in chloroform (Avanti Polar Lipids) were dried up thoroughly by nitrogen gas to form thin films, which were then hydrated by 50 mM boric acid buffer, pH 8.0. The hydrated phospholipids were modified by NBD-F at 65°C for 1 min. The reaction was stopped by cooling on ice. The labeled phospholipids, including crude NBD-PE, were extracted according to the methods reported previously (Ichihara et al., 2011). In brief, methyl *tert*-butyl ether and methanol were added to the sample (2:1:2 vol/vol) and subjected to a low-speed centrifuge. The resulting upper layer was transferred to new test tubes, dried by a nitrogen stream, and then dissolved in TBS300 to be hydrated. The hydrated crude NBD-PE was mixed with the cell extracts containing free Mdm12 or Mmm1s-Mdm12. Proteins loaded with NBD-PE were purified by the protein purification procedures described in the Protein expression, purification, and modification section.

Liposome flotation

Phospholipids were obtained from Avanti Polar Lipids except for milk PE from Nagara Science. Lipids in stock solutions in chloroform were

mixed at a desired molar ratio, and the solvent was evaporated. The lipid film was hydrated in appropriate buffer. The lipid suspension was incubated at room temperature for 30 min and extruded through polycarbonate 0.1-µm filter using a miniextruder (Avanti Polar Lipids) to prepare liposomes.

The liposome flotation assay was performed as described previously (Krick et al., 2012), with minor modifications. In brief, liposome/protein mixture was put into 5 ml of an ultracentrifuge tube and mixed with 750 µl TBS150 containing 80% (wt/vol) Nycodenz AG (Axis-Shield). The mixture was subsequently overlaid by 750 µl TBS150 containing 30% (wt/vol) Nycodenz and then 450 µl TBS150 without Nycodenz (Fig. 4, A and D). For competition experiments, the mixture was overlaid by 1,000 µl TBS150 containing 15% (wt/vol) sucrose, 1,000 µl TBS containing 7.5% (wt/vol) sucrose, and by 1,000 µl TBS150 without sucrose (Fig. 4 C). After centrifugation at 276,000 *g* for 1.5 h, fractions were collected from the top, and each fraction was analyzed for NBD fluorescence or protein amounts.

Lipid extraction and lipid transfer assay

To monitor lipid extraction from liposomes by KlMdm12 or Mmm1s–Mdm12, 10 µM protein was mixed with 200 µM donor liposome, whose lipid composition is egg PC (840051C; Avanti)/NBD-PE (L-α-phosphatidylethanolamine-*N*-[7-nitro-2-1,3-benzoxadiazol-4-yl], 810118C; Avanti = 80/20), in 150 µl TBS150 and incubated at 37°C for 30 min. The NBD-PE used here is a chicken egg PE derivative containing a head group with an NBD group and acyl chains of 18:1 and 16:0 predominantly. After incubation, the reaction mixtures were diluted with 600 µl ice-cold TBS150 and subjected to liposome flotation (described in the Liposome flotation section). After ultracentrifugation, protein-containing fractions were analyzed for fluorescence excited at 470 nm and observed at 537.5 nm with a F-2100 spectrofluorometer (Hitachi). For liposome competition experiments, 200 µM donor liposomes in 200 µl TBS150 was incubated with 10 µM Mmm1s–HMdm12 in the presence or absence of 200 µM competitor liposomes (PC/PE = 100/0 or 50/50; PE is from milk; Nagara Science) at 37°C for 30 min. Minor fluorescence contribution by the liposome to protein fractions was subtracted. Total NBD fluorescence was estimated from the fluorescence intensity of the NBD-PE–loaded liposomes solubilized with 0.1% Triton X-100.

To monitor lipid transfer from proteins to liposomes, proteins preloaded with 20 µM NBD-PE (see Preparation of proteins preloaded with NBD-PE) were mixed with 400 µM acceptor liposomes containing egg PC alone in TBS150 and incubated at 37°C for 30 min. After incubation, 150 µl of reaction mixture was diluted with 600 µl ice-cold TBS150 and subjected to liposome flotation (described above). After ultracentrifugation, every 250-µl fraction from the top was collected and mixed with 250 µl TBS150 containing 0.2% Triton X-100 for NBD fluorescence measurements.

To monitor lipid transfer between liposomes via the HMmm1s–Mdm12 complex and MBP-HMmm1s, we adopted fluorescent dequenching assays as described previously (Connerth et al., 2012; Watanabe et al., 2015; Miyata et al., 2016). The lipid compositions of the donor liposomes and acceptor liposomes are egg PC/milk PE/egg Liss-Rhod-PE (810146C; Avanti)/NBD-PE (810118C; Avanti) = 50/40/2/8 and egg PC/milk PE = 50/50, respectively. 12.5 µM donor liposomes was incubated with 50 µM acceptor liposomes in the presence or absence of the indicated proteins in 600 µl assay buffer (20 mM Tris-HCl, pH 7.5, and 150 mM NaCl) at room temperature. For NBD-PS transfer assays, NBD-PE in the aforementioned assays was replaced with NBD-PS (1,2-dioleoyl-sn-glycero-3-phospho-L-serine-*N*-(7-nitro-2-1,3-benzoxadiazol-4-yl; 810198; Avanti). The increase in dequenched NBD fluorescence was monitored using a F-2100 spectrofluorometer (Hitachi).

In vitro phospholipid transport assays were performed according to the method described previously (Kojima et al., 2016). For preparation of HMFs, the *mmm1*Δ and *mdm12*Δ strains used here (Tamura et al., 2012) were cultured on synthetic media containing lactate as a carbon source to eliminate ρ^0 or ρ^- strain before membrane isolation. HMFs were isolated from *mmm1*Δ cells expressing Vps13-D716H from the pRS314 plasmid under the control of the *GPD* promoter with wild-type Mmm1 or mutant Mmm1s in the *mmm*1Δ strain or wild-type Mdm12 or mutant Mdm12s in the *mdm*12Δ strain from the pRS316 plasmid with its own promoter, which were cultivated in SCD medium at 30°C for 15 h (Kojima et al., 2016).

Cross-linking

For in vitro cross-linking, the Mdm12–Mmm1s complex was prepared as follows. The DNA fragment for KlaMdm12(1–239) or its I5C mutant was cloned into the pET-22b vector to make a fusion protein with the TEV protease cleavage site followed by the His_{10} tag at the C terminus and that for KlaMmm1(179–434) into the pRSF-1b vector. The *E. coli* BL21(DE3) strain was transformed with those plasmids. Wild-type and I5C mutant of Mdm12 complexed with Mmm1s was expressed and purified from the *E. coli* BL21(DE3) strain transformed with those plasmids with the same procedure used for the other Mdm12–Mmm1s complexes. Purified Mdm12–Mmm1s complexes were mixed with a 5 M excess of 4-*N*-maleimidobenzophenone (NMBP; Sigma) in the presence of 1 mM tris(2-carboxyethyl)phosphine and incubated for 2 h at room temperature under dark conditions. The reaction was stopped by the addition of 5 mM DTT, and the proteins were separated from the reagents by gel-filtration chromatography. The NMBP-modified Mdm12(I5C)–Mmm1s complex was transferred to a 96-well dish and subjected to UV irradiation for 15 min on ice. The cross-linked products were analyzed by SDS-PAGE followed by immunoblotting.

Simulation methods

We performed MD simulations for two systems using the AMBER12 program package (Case et al., 2005). One is the simulation of Mdm12 including a 1-palmitoyl-2-oleyl-sn-glycero-3-phosphocholine (POPC) molecule and explicit water molecules, and the total number of atoms was 52,280. Another is that of only Mdm12 with explicit water molecules, and the total number of atoms was 52,221. Here, 16 Na^+ ions were included for each system to neutralize the systems. The force fields were AMBER ff99SB (Hornak et al., 2006), Lipid11 (Skjevik et al., 2012), and TIP3P water model (Jorgensen et al., 1983) for Mdm12, POPC, and explicit water molecules, respectively. Initial structures were built using the LEaP module in AmberTools (Case et al., 2005) and then minimized and equilibrated in three stages: heating for 200 ps from 10 K to 300 K with heavy atom positional restraints of strength 10 kcal mol^{-1} $Å^{-2}$, equilibration for 5 ns with the restraints, and equilibration for 40 ns without restraints. After that, the production runs for each system were performed for 120 ns. The MD simulations under the isobaric-isothermal ensemble with periodic boundary conditions using particle mesh Ewald method (Darden et al., 1993) to treat long-range electrostatics and a real space cutoff of 12 Å. Temperature was controlled with a Langevin thermostat with a collision frequency of 1 ps^{-1}. Pressure regulation was achieved with isotropic position scaling, a Berendsen barostat (Berendsen et al., 1984) of ∼1 atm, and a pressure relaxation time of 1 ps. Bonds involving hydrogen were constrained using the SHAKE algorithm (Ryckaert et al., 1977).

Online supplemental material

Fig. S1 shows the sequence alignment with secondary structures of Mdm12 proteins and E-SYT2. Fig. S2 documents diagrams of the

Mdm12 and Mmm1 derivatives used in this study. Fig. S3 shows the comparison of the structures of KlMdm12 derivatives, indicating that they are essentially similar, and compares the structures of KlMdm12 with that of ScMdm12. Fig. S4 compares the structures of KlMdm12 with and without phospholipid. Although lipid-free KlMdm12 exhibits more structure flexibility, the size and shape of the lipid-binding pocket do not differ significantly between lipid-bound and lipid-free KlMdm12. Fig. S5 shows the results of in vitro phospholipid transport assays using HMFs containing the ER and mitochondrial membranes with various Mmm1 or Mdm12 mutants.

Acknowledgments

We thank the members of the T. Endo laboratory for discussions and critical comments on the manuscript. We also thank Drs. Kaori Yunoki and Chika Saito for technical assistance. The synchrotron radiation experiments were performed at beam lines BL38B1 and BL44XU at SPring-8, Japan, with the approval of the Japan Synchrotron Radiation Research Institute (proposals 2012B1092 and 2013A1032).

This work was supported by Japan Society of the Promotion of Science Grants-in-Aid for Scientific Research (25840020 and 17K18230 to S. Kawano, 15H05595 to Y. Tamura, and 15H05705 and 2222703 to T. Endo), Japan Science and Technology Agency/Core Research for Evolutional Science and Technology (grant JPM JCR12M1 for T. Endo), the Swiss National Science Foundation (H. Riezman), and the National Centre of Competence in Research Chemical Biology (H. Riezman). R. Kojima was a Research Fellow of the Japan Society of the Promotion of Science.

The authors declare no competing financial interests.

Author contributions: S. Kawano and T. Endo designed the research and wrote the paper. Y. Tamura designed a part of the research and wrote the paper. S. Kawano performed most experiments, and Y. Tamura and R. Kojima performed a portion of the experiments (except for lipid analyses and MD calculations). S. Bala and E. Asai prepared materials. B. Kornmann and H. Riezman designed and A.H. Michel and I. Riezman performed experiments for lipid analyses of *S. cerevisiae* Mdm12. For MD simulations, Y. Sakae and Y. Okamoto designed and Y. Sakae performed the computations.

Submitted: 18 April 2017
Revised: 6 November 2017
Accepted: 1 December 2017

References

Adams, P.D., P.V. Afonine, G. Bunkóczi, V.B. Chen, I.W. Davis, N. Echols, J.J. Headd, L.-W. Hung, G.J. Kapral, R.W. Grosse-Kunstleve, et al. 2010. PHENIX: a comprehensive Python-based system for macromolecular structure solution. *Acta Crystallogr. D Biol. Crystallogr.* 66:213–221. https://doi.org/10.1107/S0907444909052925

AhYoung, A.P., J. Jiang, J. Zhang, X. Khoi Dang, J.A. Loo, Z.H. Zhou, and P.F. Egea. 2015. Conserved SMP domains of the ERMES complex bind phospholipids and mediate tether assembly. *Proc. Natl. Acad. Sci. USA.* 112:E3179–E3188. https://doi.org/10.1073/pnas.1422363112

Berendsen, H.J.C., J.P.M. Postma, W.F. van Gunsteren, A. DiNola, and J.R. Haak. 1984. Molecular dynamics with coupling to an external bath. *J. Chem. Phys.* 81:3684–3690. https://doi.org/10.1063/1.448118

Berger, K.H., L.F. Sogo, and M.P. Yaffe. 1997. Mdm12p, a component required for mitochondrial inheritance that is conserved between budding and fission yeast. *J. Cell Biol.* 136:545–553. https://doi.org/10.1083/jcb.136.3.545

Bhattacharya, D., and J. Cheng. 2013. 3Drefine: consistent protein structure refinement by optimizing hydrogen bonding network and atomic-level energy minimization. *Proteins.* 81:119–131. https://doi.org/10.1002/prot.24167

Bokoch, M.P., Y. Zou, S.G. Rasmussen, C.W. Liu, R. Nygaard, D.M. Rosenbaum, J.J. Fung, H.J. Choi, F.S. Thian, T.S. Kobilka, et al. 2010. Ligand-specific regulation of the extracellular surface of a G-protein-coupled receptor. *Nature.* 463:108–112. https://doi.org/10.1038/nature08650

Brünger, A.T., P.D. Adams, G.M. Clore, W.L. DeLano, P. Gros, R.W. Grosse-Kunstleve, J.S. Jiang, J. Kuszewski, M. Nilges, N.S. Pannu, et al. 1998. Crystallography & NMR system: A new software suite for macromolecular structure determination. *Acta Crystallogr. D Biol. Crystallogr.* 54:905–921. https://doi.org/10.1107/S0907444998003254

Burgess, S.M., M. Delannoy, and R.E. Jensen. 1994. MMM1 encodes a mitochondrial outer membrane protein essential for establishing and maintaining the structure of yeast mitochondria. *J. Cell Biol.* 126:1375–1391. https://doi.org/10.1083/jcb.126.6.1375

Case, D.A., T.E. Cheatham III, T. Darden, H. Gohlke, R. Luo, K.M. Merz Jr., A. Onufriev, C. Simmerling, B. Wang, and R.J. Woods. 2005. The Amber biomolecular simulation programs. *J. Comput. Chem.* 26:1668–1688. https://doi.org/10.1002/jcc.20290

Collaborative Computational Project, Number 4. 1994. The CCP4 suite: programs for protein crystallography. *Acta Crystallogr. D Biol. Crystallogr.* 50:760–763. https://doi.org/10.1107/S0907444994003112

Connerth, M., T. Tatsuta, M. Haag, T. Klecker, B. Westermann, and T. Langer. 2012. Intramitochondrial transport of phosphatidic acid in yeast by a lipid transfer protein. *Science.* 338:815–818. https://doi.org/10.1126/science.1225625

Darden, T., D. York, and L. Pedersen. 1993. Particle mesh Ewald: An N·log(N) method for Ewald sums in large systems. *J. Chem. Phys.* 98:10089–10092. https://doi.org/10.1063/1.464397

Dimmer, K.S., S. Fritz, F. Fuchs, M. Messerschmitt, N. Weinbach, W. Neupert, and B. Westermann. 2002. Genetic basis of mitochondrial function and morphology in *Saccharomyces cerevisiae*. *Mol. Biol. Cell.* 13:847–853. https://doi.org/10.1091/mbc.01-12-0588

Elbaz-Alon, Y., E. Rosenfeld-Gur, V. Shinder, A.H. Futerman, T. Geiger, and M. Schuldiner. 2014. A dynamic interface between vacuoles and mitochondria in yeast. *Dev. Cell.* 30:95–102. https://doi.org/10.1016/j.devcel.2014.06.007

Elbaz-Alon, Y., M. Eisenberg-Bord, V. Shinder, S.B. Stiller, E. Shimoni, N. Wiedemann, T. Geiger, and M. Schuldiner. 2015. Lam6 regulates the extent of contacts between organelles. *Cell Reports.* 12:7–14. https://doi.org/10.1016/j.celrep.2015.06.022

Emsley, P., B. Lohkamp, W.G. Scott, and K. Cowtan. 2010. Features and development of Coot. *Acta Crystallogr. D Biol. Crystallogr.* 66:486–501. https://doi.org/10.1107/S0907444910007493

Folch, J., M. Lees, and G.H. Sloane Stanley. 1957. A simple method for the isolation and purification of total lipids from animal tissues. *J. Biol. Chem.* 226:497–509.

Frederick, R.L., J.M. McCaffery, K.W. Cunningham, K. Okamoto, and J.M. Shaw. 2004. Yeast Miro GTPase, Gem1p, regulates mitochondrial morphology via a novel pathway. *J. Cell Biol.* 167:87–98. https://doi.org/10.1083/jcb.200405100

Guan, X.L., I. Riezman, M.R. Wenk, and H. Riezman. 2010. Yeast lipid analysis and quantification by mass spectrometry. *Methods Enzymol.* 470:369–391. https://doi.org/10.1016/S0076-6879(10)70015-X

Hönscher, C., M. Mari, K. Auffarth, M. Bohnert, J. Griffith, W. Geerts, M. van der Laan, M. Cabrera, F. Reggiori, and C. Ungermann. 2014. Cellular metabolism regulates contact sites between vacuoles and mitochondria. *Dev. Cell.* 30:86–94. https://doi.org/10.1016/j.devcel.2014.06.006

Hornak, V., R. Abel, A. Okur, B. Strockbine, A. Roitberg, and C. Simmerling. 2006. Comparison of multiple Amber force fields and development of improved protein backbone parameters. *Proteins.* 65:712–725. https://doi.org/10.1002/prot.21123

Ichihara, K., K. Yoneda, A. Takahashi, N. Hoshino, and M. Matsuda. 2011. Improved methods for the fatty acid analysis of blood lipid classes. *Lipids.* 46:297–306. https://doi.org/10.1007/s11745-011-3531-7

Jeong, H., J. Park, and C. Lee. 2016. Crystal structure of Mdm12 reveals the architecture and dynamic organization of the ERMES complex. *EMBO Rep.* 17:1857–1871. https://doi.org/10.15252/embr.201642706

Joosten, R.P., T.A. te Beek, E. Krieger, M.L. Hekkelman, R.W. Hooft, R. Schneider, C. Sander, and G. Vriend. 2011. A series of PDB related databases for everyday needs. *Nucleic Acids Res.* 39:D411–D419. https://doi.org/10.1093/nar/gkq1105

Jorgensen, W.L., J. Chandrasekhar, J.D. Madura, R.W. Impey, and M.L. Klein. 1983. Comparison of simple potential functions for simulating liquid water. *J. Chem. Phys.* 79:926–935. https://doi.org/10.1063/1.445869

Kabsch, W., and C. Sander. 1983. Dictionary of protein secondary structure: pattern recognition of hydrogen-bonded and geometrical features. *Biopolymers.* 22:2577–2637. https://doi.org/10.1002/bip.360221211

Kojima, R., T. Endo, and Y. Tamura. 2016. A phospholipid transfer function of ER-mitochondria encounter structure revealed *in vitro*. *Sci. Rep.* 6:30777. https://doi.org/10.1038/srep30777

Kopec, K.O., V. Alva, and A.N. Lupas. 2010. Homology of SMP domains to the TULIP superfamily of lipid-binding proteins provides a structural basis for lipid exchange between ER and mitochondria. *Bioinformatics.* 26:1927–1931. https://doi.org/10.1093/bioinformatics/btq326

Kopec, K.O., V. Alva, and A.N. Lupas. 2011. Bioinformatics of the TULIP domain superfamily. *Biochem. Soc. Trans.* 39:1033–1038. https://doi.org/10.1042/BST0391033

Kornmann, B., E. Currie, S.R. Collins, M. Schuldiner, J. Nunnari, J.S. Weissman, and P. Walter. 2009. An ER-mitochondria tethering complex revealed by a synthetic biology screen. *Science.* 325:477–481. https://doi.org/10.1126/science.1175088

Kornmann, B., C. Osman, and P. Walter. 2011. The conserved GTPase Gem1 regulates endoplasmic reticulum-mitochondria connections. *Proc. Natl. Acad. Sci. USA.* 108:14151–14156. https://doi.org/10.1073/pnas.1111314108

Krick, R., R.A. Busse, A. Scacioc, M. Stephan, A. Janshoff, M. Thumm, and K. Kühnel. 2012. Structural and functional characterization of the two phosphoinositide binding sites of PROPPINs, a β-propeller protein family. *Proc. Natl. Acad. Sci. USA.* 109:E2042–E2049. https://doi.org/10.1073/pnas.1205128109

Lahiri, S., J.T. Chao, S. Tavassoli, A.K.O. Wong, V. Choudhary, B.P. Young, C.J.R. Loewen, and W.A. Prinz. 2014. A conserved endoplasmic reticulum membrane protein complex (EMC) facilitates phospholipid transfer from the ER to mitochondria. *PLoS Biol.* 12:e1001969. https://doi.org/10.1371/journal.pbio.1001969

Lang, A.B., A.T. John Peter, P. Walter, and B. Kornmann. 2015. ER–mitochondrial junctions can be bypassed by dominant mutations in the endosomal protein Vps13. *J. Cell Biol.* 210:883–890. https://doi.org/10.1083/jcb.201502105

Lovell, S.C., I.W. Davis, W.B. Arendall III, P.I.W. de Bakker, J.M. Word, M.G. Prisant, J.S. Richardson, and D.C. Richardson. 2003. Structure validation by Calpha geometry: phi,psi and Cbeta deviation. *Proteins.* 50:437–450. https://doi.org/10.1002/prot.10286

McCoy, A.J., R.W. Grosse-Kunstleve, P.D. Adams, M.D. Winn, L.C. Storoni, and R.J. Read. 2007. Phaser crystallographic software. *J. Appl. Cryst.* 40:658–674. https://doi.org/10.1107/S0021889807021206

Miyata, N., Y. Watanabe, Y. Tamura, T. Endo, and O. Kuge. 2016. Phosphatidylserine transport by Ups2-Mdm35 in respiration-active mitochondria. *J. Cell Biol.* 214:77–88. https://doi.org/10.1083/jcb.201601082

Murley, A., R.D. Sarsam, A. Toulmay, J. Yamada, W.A. Prinz, and J. Nunnari. 2015. Ltc1 is an ER-localized sterol transporter and a component of ER-mitochondria and ER-vacuole contacts. *J. Cell Biol.* 209:539–548. https://doi.org/10.1083/jcb.201502033

Murshudov, G.N., P. Skubák, A.A. Lebedev, N.S. Pannu, R.A. Steiner, R.A. Nicholls, M.D. Winn, F. Long, and A.A. Vagin. 2011. REFMAC5 for the refinement of macromolecular crystal structures. *Acta Crystallogr. D Biol. Crystallogr.* 67:355–367. https://doi.org/10.1107/S0907444911001314

Nguyen, T.T., A. Lewandowska, J.Y. Choi, D.F. Markgraf, M. Junker, M. Bilgin, C.S. Ejsing, D.R. Voelker, T.A. Rapoport, and J.M. Shaw. 2012. Gem1 and ERMES do not directly affect phosphatidylserine transport from ER to mitochondria or mitochondrial inheritance. *Traffic.* 13:880–890. https://doi.org/10.1111/j.1600-0854.2012.01352.x

Osman, C., C. Merkwirth, and T. Langer. 2009. Prohibitins and the functional compartmentalization of mitochondrial membranes. *J. Cell Sci.* 122:3823–3830. https://doi.org/10.1242/jcs.037655

Otwinowski, Z., and W. Minor. 1997. Processing of X-ray diffraction data collected in oscillation mode. *Methods Enzymol.* 276:307–326. https://doi.org/10.1016/S0076-6879(97)76066-X

Ryckaert, J.-P., G. Ciccotti, and H.J.C. Berendsen. 1977. Numerical integration of the cartesian equations of motion of a system with constraints: Molecular dynamics of *n*-alkanes. *J. Comput. Phys.* 23:327–341. https://doi.org/10.1016/0021-9991(77)90098-5

Šali, A., and T.L. Blundell. 1993. Comparative protein modelling by satisfaction of spatial restraints. *J. Mol. Biol.* 234:779–815. https://doi.org/10.1006/jmbi.1993.1626

Scharwey, M., T. Tatsuta, and T. Langer. 2013. Mitochondrial lipid transport at a glance. *J. Cell Sci.* 126:5317–5323. https://doi.org/10.1242/jcs.134130

Schauder, C.M., X. Wu, Y. Saheki, P. Narayanaswamy, F. Torta, M.R. Wenk, P. De Camilli, and K.M. Reinisch. 2014. Structure of a lipid-bound extended synaptotagmin indicates a role in lipid transfer. *Nature.* 510:552–555. https://doi.org/10.1038/nature13269

Skjevik, A.A., B.D. Madej, R.C. Walker, and K. Teigen. 2012. LIPID11: a modular framework for lipid simulations using amber. *J. Phys. Chem. B.* 116:11124–11136. https://doi.org/10.1021/jp3059992

Sogo, L.F., and M.P. Yaffe. 1994. Regulation of mitochondrial morphology and inheritance by Mdm10p, a protein of the mitochondrial outer membrane. *J. Cell Biol.* 126:1361–1373. https://doi.org/10.1083/jcb.126.6.1361

Stroud, D.A., S. Oeljeklaus, S. Wiese, M. Bohnert, U. Lewandrowski, A. Sickmann, B. Guiard, M. van der Laan, B. Warscheid, and N. Wiedemann. 2011. Composition and topology of the endoplasmic reticulum-mitochondria encounter structure. *J. Mol. Biol.* 413:743–750. https://doi.org/10.1016/j.jmb.2011.09.012

Tamura, Y., O. Onguka, A.E. Hobbs, R.E. Jensen, M. Iijima, S.M. Claypool, and H. Sesaki. 2012. Role for two conserved intermembrane space proteins, Ups1p and Ups2p, [corrected] in intra-mitochondrial phospholipid trafficking. *J. Biol. Chem.* 287:15205–15218. https://doi.org/10.1074/jbc.M111.338665

Tamura, Y., H. Sesaki, and T. Endo. 2014. Phospholipid transport via mitochondria. *Traffic.* 15:933–945. https://doi.org/10.1111/tra.12188

Tan, T., C. Ozbalci, B. Brügger, D. Rapaport, and K.S. Dimmer. 2013. Mcp1 and Mcp2, two novel proteins involved in mitochondrial lipid homeostasis. *J. Cell Sci.* 126:3563–3574. https://doi.org/10.1242/jcs.121244

Tatsuta, T., and T. Langer. 2017. Intramitochondrial phospholipid trafficking. *Biochim. Biophys. Acta.* 1862:81–89. https://doi.org/10.1016/j.bbalip.2016.08.006

Voss, C., S. Lahiri, B.P. Young, C.J. Loewen, and W.A. Prinz. 2012. ER-shaping proteins facilitate lipid exchange between the ER and mitochondria in *S. cerevisiae*. *J. Cell Sci.* 125:4791–4799. https://doi.org/10.1242/jcs.105635

Watanabe, Y., Y. Tamura, S. Kawano, and T. Endo. 2015. Structural and mechanistic insights into phospholipid transfer by Ups1-Mdm35 in mitochondria. *Nat. Commun.* 6:7922. https://doi.org/10.1038/ncomms8922

Yamano, K., S. Tanaka-Yamano, and T. Endo. 2010. Tom7 regulates Mdm10-mediated assembly of the mitochondrial import channel protein Tom40. *J. Biol. Chem.* 285:41222–41231. https://doi.org/10.1074/jbc.M110.163238

Youngman, M.J., A.E. Hobbs, S.M. Burgess, M. Srinivasan, and R.E. Jensen. 2004. Mmm2p, a mitochondrial outer membrane protein required for yeast mitochondrial shape and maintenance of mtDNA nucleoids. *J. Cell Biol.* 164:677–688. https://doi.org/10.1083/jcb.200308012

Yu, J., Y. Zhou, I. Tanaka, and M. Yao. 2010. Roll: a new algorithm for the detection of protein pockets and cavities with a rolling probe sphere. *Bioinformatics.* 26:46–52. https://doi.org/10.1093/bioinformatics/btp599